Effects of mineralogy on Δ_{47} and Δ_{48} of carbonate-derived CO_2 below analytical resolution

Miguel Bernecker[1,*], Magali Bonifacie[2], Philip Staudigel[1], Niels Meijer[3], Julien Siebert[2], Nicolas Wehr[2], Eiken Haussühl[1], Stefano M. Bernasconi[4], Daniel Petrash[5], Martin Dietzel[6], Jens Fiebig[1]

[1]Institut für Geowissenschaften, Goethe-Universität Frankfurt, Altenhöferallee 1, 60438 Frankfurt am Main, Germany
[2]Université Paris Cité, Institut de Physique du Globe de Paris, CNRS, F-75005 Paris, France
[3]Senckenberg Biodiversität und Klima Forschungscenter, Senckenberganlage 25, 60325 Frankfurt am Main, Germany
[4]Department of Earth and Planetary Sciences, ETH Zürich, Sonneggstrasse 5, 8092 Zürich, Switzerland
[5]Czech Geological Survey, 15200 Prague, Czechia
[6]Institute of Applied Geosciences, Graz University of Technology, Rechbauerstraße 12, Graz 8010, Austria
*Corresponding author: bernecker@em.uni-frankfurt.de

Keywords: Δ_{47}, Δ_{48}, carbonate clumped isotopes, acid fractionation factors

Abstract (max. 500)

Due to the lack of direct methods capable of determining the abundance of isotopologues containing multiple heavy isotopes within the crystal lattice, carbonates are typically reacted with phosphoric acid to produce CO_2 analyte for clumped isotope analyses. This reaction is associated with fractionations of both bulk oxygen and clumped isotopes. Accurate knowledge of the effect of cation substitution on the degree of isotopic clumping in the carbonate phase and on acid fractionation factors is crucial for accurate temperature reconstructions based on clumped isotope measurements of extracted CO_2 from various carbonate mineralogies. Previous studies have yielded contradicting results on the effect of carbonate mineralogy on both Δ_{47} acid fractionation factors and the validity of a universal Δ_{47}-T relationship, and, so far, a systematic investigation of mineralogy-specific effects on Δ_{48} is lacking.

In this study, we have analyzed the dual clumped isotope composition of stochastic and non-stochastic calcites, aragonites, dolomites, witherites, and siderites with unprecedented long-term repeatabilities (1SDs) of 8.1 and 28.1 ppm for Δ_{47} and Δ_{48}, respectively. In order to facilitate complete acid digestion of dolomite and siderite in a reasonable timeframe, an acid digestion temperature of 110°C was used for these minerals instead of the 90°C applied to calcite, aragonite and witherite. A set of calcite samples was reacted at both temperatures to determine the calcite-specific difference in acid digestion-related fractionation factors between 90 and 110°C, yielding $\Delta^*_{47,\ 110-90°C}$ = -0.0147±0.002 ‰ and $\Delta^*_{48,\ 110-90°C}$ = -0.0148±0.006 ‰ (2SEs, n=8). After projecting Δ_{47} and Δ_{48} results from stochastic dolomite and siderite to the carbon dioxide equilibrium scale (CDES90) using the calcite-specific $\Delta^*_{i,\ 110-90°C}$, calcite, aragonite, dolomite, witherite and siderite exhibit statistically

indistinguishable $\Delta_{47,\,CDES90}$ and $\Delta_{48,\,CDES90}$ values, with weighted averages of 0.1850±0.0042 ‰ and 0.1255±0.0130 ‰ (weighted 2SEs, n=15), respectively. In addition, $\Delta_{47,\,CDES90}$ and $\Delta_{48,\,CDES90}$ values of non-stochastic aragonites (n=2), (proto-)dolomites (n=2) and witherite (n=1) correspond to calcite equilibrium values predicted by their independently known formation temperatures (Fiebig et al., 2024). Natural dolomites and siderites of unknown formation temperature are also indistinguishable from the calcite equilibrium line. Overall, these results imply that calcite, aragonite, dolomite and witherite share indistinguishable Δ_{47}^{*}, Δ_{48}^{*} and Δ_{63}-Δ_{64}-T relationships. As a consequence, the calcite-specific equilibrium $\Delta_{47,\,CDES90}$-$\Delta_{48,\,CDES90}$-T relationships of Fiebig et al. (2024) can be reliably applied to aragonite, dolomite, and witherite. More precipitation experiments under controlled conditions are necessary to clarify with more confidence if these relationships are also valid for siderite.

1. Introduction

Carbonate clumped isotope analysis concerns the determination of the abundances of carbonate isotopologues in which at least two light isotopes are substituted by their heavy homologues. The Δ_i metric expresses the extent to which clumped isotopologues are enriched relative to stochastically driven partitioning of isotopes amongst isotopologues (Ghosh et al., 2006; Schauble et al., 2006; Wang et al., 2004), see Equation 1, where $R_i = \frac{\mathrm{m/z}_i}{\mathrm{m/z}_{44}}$ and R_i^{*} is the stochastically expected isotopologue abundance as determined based on the bulk isotopic composition (for i in 47, 48 and 49).

$$\Delta_i = \left(\frac{R_i}{R_i^{*}} - 1\right) \times 1000\ [‰] \qquad (1)$$

Departures from stochastic partitioning are due to the slight mass differences between isotopes and isotopologues, thus influencing molecular vibrational zero-point energies (Bigeleisen, 1965), making 'clumped' arrangements of heavy isotopes thermodynamically favorable over stochastic arrangements. Because direct determination of clumped $CaCO_3$ isotopologues from within the crystal lattice is not technically feasible, it is measured on CO_2 released from phosphoric acid digestion of the carbonate (Ghosh et al., 2006).

Since the pioneering isotope studies on carbonate minerals (McCrea, 1950; Urey, 1947), it has been shown many times that acid digestion is associated with oxygen isotope fractionation, such that the oxygen isotope composition of the evolved CO_2 ($\delta^{18}O_{CO_2}$) is enriched relative to that of the carbonate ($\delta^{18}O_{XCO_3}$). This occurs because only 2/3 of all oxygen atoms in the carbonate ion are released as CO_2, whereas 1/3 of the oxygen atoms partition into water; see Equation 2, where X is a divalent cation, e.g., Ca^{2+}, Mg^{2+}, Fe^{2+} or Ba^{2+}

$$H_3PO_4 + XCO_3 \rightarrow XHPO_4 + H_2O + CO_2 \qquad (2)$$

Sharma and Clayton (1965) have already demonstrated differences in oxygen isotope fractionation factors associated with acid digestion (${}^{18}\alpha_{CO_2\text{-}XCO_3}$; Equation 3) for different carbonate minerals

$$ {}^{18}\alpha_{CO_2\text{-}XCO_3} = \frac{(\delta^{18}O_{CO_2} + 1000)}{(\delta^{18}O_{XCO_3} + 1000)} \quad (3) $$

Follow-up studies have progressively applied more advanced methodologies and empirically tested a variety of carbonate minerals, thus confirming mineral-specific ${}^{18}\alpha_{CO_2\text{-}XCO_3}$ (e.g., Böttcher, 1996; Gilg et al., 2003; Kim & O'Neil, 1997; Rosenbaum & Sheppard, 1986). It has been shown that the extent of acid fractionation is affected by acid temperature (McCrea, 1950), acid concentration (Wendeberg et al., 2011), reaction time and technique (Swart et al., 1991), carbonate crystal structure (i.e., rhombohedral calcite group vs. orthorhombic aragonite group; Gilg et al., 2003; Sharma & Clayton, 1965), different cation substitutions (Guo et al., 2009), as well as the grain size of reacted carbonate powders (Swart et al., 1991; Walters et al., 1972).

As observed for bulk oxygen isotopes, the clumped isotope compositions of CO_2 (Δ_{47}, Δ_{48} and Δ_{49}) are likewise offset by acid fractionation factors (i.e., Δ^*_{47}, Δ^*_{48} and Δ^*_{49}) from those of XCO_3 precursor molecules within the crystal lattice (Δ_{63}, Δ_{64} and Δ_{65}, respectively) (e.g., Guo et al., 2009):

$$ \Delta_{47} = \Delta_{63} + \Delta^*_{47}\ [‰] \quad (4) $$

$$ \Delta_{48} = \Delta_{64} + \Delta^*_{48}\ [‰] \quad (5) $$

$$ \Delta_{49} = \Delta_{65} + \Delta^*_{49}\ [‰] \quad (6) $$

Clumped isotope acid fractionation factors Δ^*_i (AFFs), therefore describe the extent to which bonds between light isotopes are preferentially broken over those of heavy isotopes during acid digestion of carbonates. The magnitude of these AFFs depends on reaction temperature (e.g., Guo et al., 2009; Defliese et al., 2015), and possibly on mineralogy (e.g., Guo et al., 2009), with $\Delta^*_{i,\,T1-T2\,°C}$ representing the difference between temperatures T1 and T2 in °C for a given mineralogy. The evolved CO_2 gas is enriched in heavy isotopologues, when compared to the initial $CaCO_3$ phase (Ghosh et al., 2006). Direct determination of Δ^*_i can be achieved through analysis of CO_2 derived from phosphoric acid digestion of samples that are characterized by stochastic distribution of isotopes amongst carbonate isotopologues, i.e., Δ_{63}, Δ_{64}, and Δ_{65}= 0‰ (Schauble et al., 2006; Hill et al., 2014). For the identification of the effects of cation substitution and crystal structure on Δ_{63}, Δ_{64} and Δ_{65} values, additional analysis of samples of non-stochastic composition and known formation temperatures is required, since equilibrium Δ_{63}-Δ_{64}-Δ_{65} values may have mineralogy-dependent temperature sensitivities.

Schauble et al. (2006) and Hill et al. (2014) have calculated equilibrium constants for individual CO_3^{2-} groups using first-principles lattice dynamics. These predicted that aragonite, calcite, dolomite and witherite differ in their intrinsic Δ_{63}-T relationships by up to 30 ppm. Theoretical cluster modeling by Guo et al. (2009) indicated additional cation-dependent differences of ≤30 ppm in AFFs for aragonite, calcite, witherite and dolomite. Predicted combined differences make up ≤50 ppm of absolute variation in Δ_{47}-T relationships between carbonate mineralogies at 25°C acid reaction temperatures (Guo et al., 2009). Considering that Δ^*_{47}

decreases with increasing acid digestion temperature, this value may represent an upper estimate of the Δ_{47} difference that can be expected.

Empirical studies on aragonite and calcite implied that both mineralogies share indistinguishable Δ_{47}^{*} and Δ_{63}-T relationships (Defliese et al., 2015; Wacker et al., 2013). These findings were confirmed in a more recent study (de Winter et al., 2022) utilizing updated IUPAC parameters (Daëron et al., 2016; Schauer et al., 2016) and carbonate-based standardization (Bernasconi et al., 2021). Discrepant results were reported when calcite was compared to dolomite. Some early investigations revealed dolomite-specific Δ_{47}^{*} (Müller et al., 2017; Murray et al., 2016), whereas others reported no resolvable differences in Δ_{47}^{*} and/or Δ_{47}-1/T relationships between dolomite and calcite (Bonifacie et al., 2017; Defliese et al., 2015; Winkelstern et al., 2016). The most recent study by Anderson et al. (2024), who considered IUPAC parameters and carbonate-based standardization, supported the hypothesis that dolomite and calcite share common Δ_{47}^{*} and Δ_{47}-T relationships.

New generations of mass spectrometers have improved Δ_{47} repeatability by a factor of ca. 2-3 compared to the previously described studies. This is due to the improvements in the suppression of secondary electrons which otherwise would lead to a negative bias in mass signals (commonly referred to as pressure baseline, PBL), and the utilization of high-ohmic Faraday cups including a m/z 47.5 half-mass cup for continuous PBL monitoring (Fiebig et al., 2019). Additionally, investigation of Δ_{48} simultaneously to Δ_{47} with long-term repeatabilities approaching theoretical shot-noise limits became possible (Bernecker et al., 2023; Fiebig et al., 2019). Through these so-called “dual clumped” isotope measurements, the effect and relevance of rate-limiting kinetics on the clumped and bulk isotopic compositions of natural carbonates could be identified (Bajnai et al., 2020; Fiebig et al., 2019). Archives characterized by Δ_i values that are not solely controlled by precipitation temperature include warm- and cold-water corals (Davies et al., 2022), brachiopods (Davies et al., 2023), authigenic methane seep carbonates (Staudigel et al., 2024), and eggshell calcite of birds (Tagliavento et al., 2023). With these improvements, even a temperature trend for Δ_{49} has been resolved (Bernecker et al., 2023).

Currently, there is no study available that has investigated the effect of cation substitution on the Δ_{48} value of the CO_2 extracted from carbonates. We have analyzed aragonite, calcite, dolomite, siderite and witherite samples, both of known “cold” formation temperature, and re-ordered at ≥800°C, using the latest high-precision technology (Bernecker et al., 2023) to investigate potential differences in Δ_{47}^{*}, Δ_{48}^{*} and Δ_{63}-Δ_{64}-1/T relationships between these carbonate mineralogies. We demonstrate that aragonite, calcite, dolomite, and witherite reacted at temperatures ≥90°C share indistinguishable Δ_{47}^{*}, Δ_{48}^{*} and Δ_{47}-Δ_{48}-T equilibrium relationships.

2. Methods

2.1 Samples

Sample material was crushed using mortar and pestle, sieved using a 200 µm mesh sieve before stored in a 30°C vacuum dry oven and finally weighed out into Ag-capsules to be loaded into the autosampler for dual clumped isotope analysis.

2.1.1 Samples heated to temperatures ≥800°C

Samples of aragonite, calcite, dolomite, siderite and witherite were re-ordered at temperatures between 800 and 1200°C, through piston cylinder experiments (Section 2.2). Temperature and pressure were conditioned to match the respective stability fields of these mineralogies (Table 1). Additionally, we re-analyzed **ETH-1-1100** and **ETH-2-1100**, which were already utilized for the dual clumped isotope calibration of Fiebig et al. (2021; 2024). These two samples (former ETH-1 and ETH-2, respectively; Bernasconi et al., 2018; 2021) were heated to 1,100±10°C at 200 MPa for 24 h. Aragonite sample **Bilin 1(H)**, originally investigated by Müller et al. (2017), was heated to 850°C at 3.5 GPa for 4 h.

Table 1: Piston cylinder samples and experimental conditions. †Unknown heating duration; temperature remained at 800°C for at least 2 h before sample was quenched.

Acid temp. (°C)	**Sample**	**Temp.** (°C)	**Duration** (h)	**Pressure** (GPa)	**Mineralogy**	**Reference**
90	Bilin 1(H)	850	4	3.5	Aragonite	Müller et al. (2017)
90	Arag2-800	800	48	3		This study
90	Arag1-800	800	72	3		
110	Dolo2_800	800	48	2.5	Dolomite	
110	Dolo1_1200	1,200	53	1.5		
110	Sid_800	800	64	3	Siderite	
90	DIC3-800	800	72	2	Witherite	
90	DIC1-1100	1,100	40	2.3		
90	DIC1-800	800	72	2		
90	*ETH-1-800*	*†800*	*†48*	*†1*	Calcite	
90	MERCK-800	800	48	1		
90	ETH-2-800	800	72	1		
90 + 110	ETH-1-1100	1,100	24	0.2		Fiebig et al. (2021, 2024)
90	ETH-2-1100	1,100	24	0.2		

2.1.2 Non-heated samples of colder formation temperatures

Dual clumped isotope analyses were carried out on a suite of synthetic and natural carbonate minerals of both known and unknown formation temperatures (Table 2).

Two modern aragonitic bivalve mollusk shells were examined. These were cultured under controlled temperatures. Sample **AI_006** (*Arctica islandica)* was cultured at NIOZ (Texel, NL) at 12°C. **RM1** represents the shell of *M modiolus*, which was collected at low tide from a beach in Tentsmuir Forest, southeast Scotland in 2020. The World Ocean Atlas (WOA) lists a mean annual temperature of 9.7°C and a seasonal amplitude of 6-14°C for the site of collection.

Dolomite calibration samples **Dolomite_350A-9** (dolomitized calcite) and **Dolomite_80-1** (direct precipitation) of known experimental temperatures (351.4±2 and 80.2±2°C, respectively) were originally described in detail by Horita (2014) and were later analyzed for their Δ_{47}-T relationships (Anderson et al., 2024; Bonifacie et al., 2017). **Dolomite_BE** constitutes a natural low-temperature (25±4°C) dolomite, precipitated in a shallow (<0.5 m), hypersaline lagoon near Rio de Janeiro (Bonifacie et al., 2017). **IPGP-SRM88-1** and **IPGP-INYO** are dolomite samples of unknown formation temperature, originating from a batch utilized as in-house standard at the clumped isotope laboratory at IPGP, the latter of which has been analyzed for Δ_{47} by Anderson et al. (2024). A suite of dolomite samples originates from a diagenetically overprinted lacustrine section of the Eger Graben, and is Miocene (Burdigalian) in age (Rojik, 2004) Dolomitic samples **D-Mio** originate from dolomite-bearing claystone and were taken at different depths from the ca. 70 m thick (top-eroded) Cypris Formation, Sokolov sub-basin (core Dp-333 at CGS core repository). Temperature estimates derived from a mean random vitrinite reflectance of 0.211 ± 0.03 for low thermal maturity organic matter (Kříbek et al., 2017) indicate that the burial temperature experienced by this lithology was below 60°C.

Siderite samples **Sid_D1-Sid_D5** are sub-samples of a 45 cm diameter siderite concretion retrieved from palustrine deposits within the basal member of the Early Miocene Most Formation (Bilina Mine, Ústí nad Labem Region, Czech Republic). The alteration aureole surrounding this concretion in the host rock is represented by **Sid_D6**. **IPGP-Sid1** is a pure siderite from the La Mûre deposit in France, and has already been investigated for its bulk isotopic composition (Lebeau et al., 2014).

DIC1 represents a synthetic witherite sample, that has been precipitated by slow addition of saturated $BaCl_2$ to an isotopically equilibrated 0.1M $NaHCO_3$ solution. Both solutions were produced using the same MilliQ water and thermally equilibrated at 25°C. Addition of $BaCl_2$ was stopped after 5 % of the DIC pool had been removed through $BaCO_3$ precipitation. $BaCO_3$ was removed from the solution by filtration, rinsed twice with MilliQ water, and finally dried at 25°C.

Table 2: Non-heated aragonite, dolomite, siderite and witherite samples of un-/controlled formation temperatures.

Acid reaction temperature	Sample	Temp. (°C)	Mineralogy	Reference
90	DIC1	25.0	Witherite	This study
90 + 110	RM1	9.7	Aragonite	
90	AI_006	12.0		
110	Dolomite_350A-9	351.4	Dolomite	Bonifacie et al. (2017)
110	Dolomite_BE	25.0		
110	Dolomite_80-1	80.2		
110	IPGP-SRM88-1	-		This study
110	IPGP-INYO	-		Anderson et al. (2024)
110	D-Mio-1798_110C	-		This study
110	D-Mio-3010_110C	-		
110	D-Mio-3016_110C	-		
110	D-Mio-3056_110C	-		
110	D-Mio-474_110C	-		
110	D-Mio-5520_110C	-		
110	IPGP-SID1	-	Siderite	Lebeau et al. (2014)
110	Sid_D1	-		This study
110	Sid_D2	-		
110	Sid_D3	-		
110	Sid_D4	-		
110	Sid_D5	-		
110	Sid_D6	-		

2.2 Piston cylinder experiments

Heating experiments on different carbonate materials were carried out in piston cylinders at 800-1,200°C for 2-3 days (Table 1) in the Cosmochemistry, Astrophysics and Experimental Geophysics (CAGE) Laboratory at the Institut de Physique du Globe de Paris (IPGP) following the setup and methods outlined by Siebert et al. (2011). The starting sample was placed in a ¾" or ½" diameter welded platinum capsule and then in a pressure-transmitting medium (here Talc-Pyrex) to ensure good thermal insulation and hydrostatic containment of the samples.

The temperature was measured by a W/Re thermocouple located just above the capsule. After having reached the targeted conditions (Table 1), samples were quenched very fast (ca. 500°C/s). In all cases, samples were cooled from equilibration temperature to 200°C in less than 3 s, and to room temperature in around 1 min. Uncertainties are less than 50°C for temperature and around 0.1 GPa for pressure.

2.3 XRD

Powder x-ray diffraction (XRD) analyses were carried out in the Crystallography/Mineralogy Laboratory of Goethe University Frankfurt am Main, Institute of Geosciences (GU) and at IPGP.

XRD analyses at GU were performed on a X-PertPro diffractometer equipped with a linear position-sensitive detector from PANalytical (PIXcel3D) and a Johannson monochromator (Ge 111) using Cu Kα1 radiation and fixed divergence slits. Samples were analyzed in the 5-125° range utilizing a step size of 0.0032826° at 549 s integration time per step. The powder was applied on a silicon single-crystal plate.

XRD measurements at IPGP were carried out on an Empyrean diffractometer (Malvern-Panalytical), equipped with a copper tube (kα=1.541874 Å) and a PIXcel multichannel detector in capillary configuration. A focusing x-ray mirror was placed in the incident beam path. The angular range was varied from 10 to 80°, with a step size of 0.0131° and a counting time of 40 s.

2.4 Mass spectrometry

2.4.1 Experimental setup

Bulk stable and dual clumped isotope analyses were carried out at the Stable Isotope Laboratory at GU following the methodology of Bernecker et al. (2023). Determination of $\delta^{13}C$, $\delta^{18}O$, Δ_{47}, Δ_{48} and Δ_{49} is achieved using a Thermo Scientific 253plus gas-source isotope ratio mass spectrometer attached to Hofmann's Auto Line (HAL, Fiebig et al., 2019). Separate analytical sessions were conducted for acid reaction temperatures of 90 and 110°C. Each replicate was measured in at least 13 acquisitions, which were defined by 10 cycles of 20 s integration time each, yielding a minimum total integration time of 2,600 s per replicate. Initial m/z 44 signal intensities for reference and sample gas were adjusted to 16,000 ± 100 mV for each acquisition. The CO_2 working gas composition on this setup is $\delta^{13}C_{VPDB}$ = -4.21 ‰ and $\delta^{18}O_{VSMOW}$ = 25.26 ‰. $\delta^{13}C_{CO_2}$ and $\delta^{18}O_{CO_2}$ values of unknown samples are reported relative to VSMOW, after normalizing to CO_2 extracted from calcite standards ETH-1 and ETH-2, considering nominal $\delta^{13}C_{calcite}$ and $\delta^{18}O_{calcite}$ values of Bernasconi et al. (2018) and the ${}^{18}\alpha_{CO_2\text{-}calcite}$ at 90°C after Kim et al. (2007). Since the focus of this study is on clumped isotopes, we do not account for differences in ${}^{18}\alpha_{CO_2\text{-}XCO_3}$ between carbonate mineralogies and reaction temperatures.

2.4.2 Acid reaction temperature and time needed for quantitative digestion of carbonates in a common acid bath

Modern routine setups typically perform reactions at temperatures over 70°C for calcites, with continuous cryogenic removal of CO_2, thereby minimizing the time of CO_2-acid interaction (e.g., Bernasconi et al., 2021). At GU, pressure inside the extraction volume up to the first CO_2 trap is monitored during acid digestion and CO_2 extraction (HAL, Fiebig et al., 2019). For calcitic and aragonitic samples, we generally react 10±0.2 mg material per replicate

at 90°C acid temperature for 30 min in a magnet bar-stirred common acid bath (CAB). Reaction usually finishes within 10-15 min, when a minimum baseline pressure is asymptotically reached (Figure 1a, b). The same behavior is observed for witherite (Figure 1c) using 19.8±0.2 mg of sample material per replicate, in order to produce the same amount of CO_2 analyte.

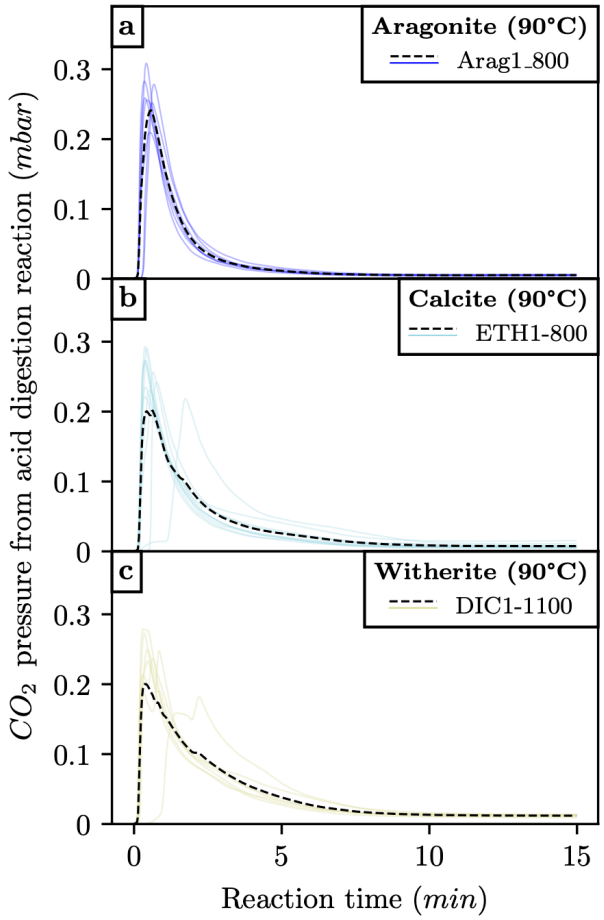

Figure 1: CO_2 pressure evolving through acid digestion reactions at 90°C for a) aragonite, b) calcite and c) witherite. Colored thin lines represent individual replicates, the black dashed lines display average CO_2 yields for a given sample.

Pressure monitoring revealed that a reaction time of 60 min at 90°C is not sufficient to react all dolomite and siderite samples quantitatively. After this period, gas bubbles were not visible anymore, but pressure still evolved non-asymptotically (Figure 2), unlike in calcite, aragonite and witherite reactions (Figure 1). An asymptotic return to minimum pressure values only occurred after increasing the reaction temperature to 110°C, using reaction times of 60 and 120 min for dolomite and siderite, respectively (Figure 3). We monitored the pressure in trap 2 (HAL, Fiebig et al., 2019) and ensured quantitative yields (with mineralogy-dependent weights corresponding to 100 µmol CO_2), before analyte CO_2 was entrained at -80°C into the He-carrier gas for GC purification.

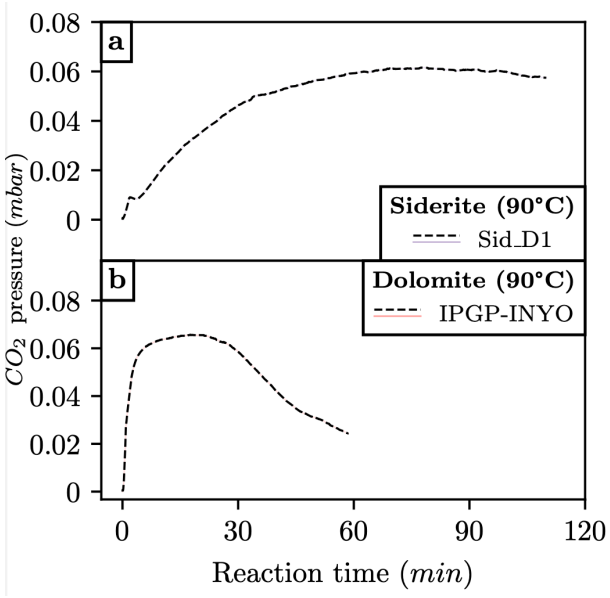

Figure 2: CO_2 pressure evolving through acid digestion reaction at 90°C for a) siderite and b) dolomite.

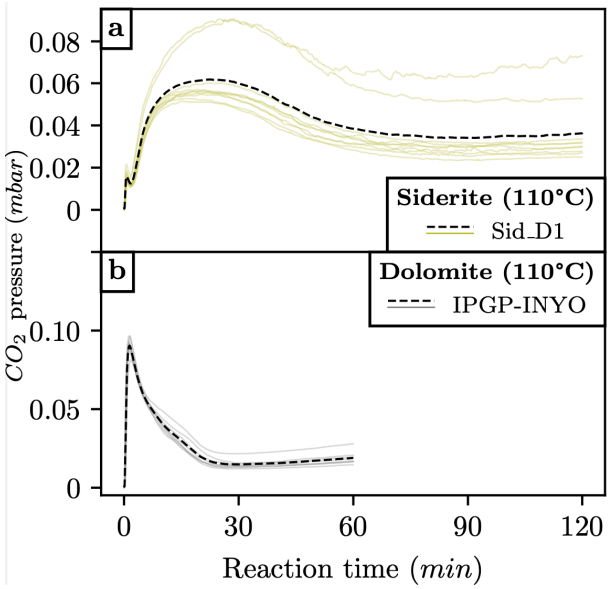

Figure 3: CO_2 pressure evolving through acid digestion reaction at 110°C for a) siderite and b) dolomite. Colored thin lines represent individual replicates, whereas the black dashed lines display average CO_2 yields for a given sample.

Slow, but steadily increasing pressure after the dolomite reactions had finished are due to helium leaking into the reaction chamber. For siderite samples, H_2 formed through oxidation of Fe^{2+} to Fe^{3+} within the acid (Crouzet et al., 2017) is a possible contributor to this elevated final pressure. Because both of these sources of pressure are non-condensable in liquid nitrogen, they are effectively removed during sample gas purification.

2.4.3 Data processing

Analytical data was treated following the processing scheme outlined by Bernecker et al. (2023). In short, raw intensity data was corrected for a PBL effect after determination of optimized scaling factors considering sets of gas standards of different bulk isotopic compositions, equilibrated at 25 or 1,000°C (Bernecker et al., 2023; Fiebig et al., 2021). In a next step, baseline-corrected δ^{45}-δ^{49} values were used to perform equilibrated gas-based standardization using nominal theoretical CO_2 equilibrium Δ_{47} (Petersen et al., 2019) and Δ_{48} (Wang et al., 2004; Fiebig et al., 2019) values for CO_2 equilibrated at 25°C and 1000°C and the D47crunch methodology of Daëron (2021), which considers variance minimization of unknowns and anchors. ETH-1, ETH-2, ETH-3 (Bernasconi et al., 2021), ETH-3oxi (Fiebig et al., 2024), Carrara and GU1 (Fiebig et al., 2021) were routinely analyzed along with sample unknowns to account for long-term drifts. Non-bleached replicates of ETH-3 (Bernasconi et al., 2021) were excluded from the variance minimization algorithm of D47crunch (Daëron, 2021) as it has been shown that their Δ_{47} and Δ_{48} values were compromised by variable amounts of NO_2 interferent (Fiebig et al., 2024).

For the determination of $\Delta_{i,\,CDES90}$ and $\Delta_{i,\,CDES110}$ values of unknown samples, D47crunch's *pooled session* processing scheme was applied considering data from all sessions, i.e., not distinguishing between sessions carried out at reaction temperatures of 90 or 110°C. This does not introduce any bias in measured Δ_i values through the variance minimization algorithm inherent to the pooled approach, provided a given carbonate replicate is identified by its sample name *and* reaction temperature. Note that Δ_i values of equilibrated gases are not affected by the acid. Equilibrated gases are only introduced into the gas purification system of HAL after the acid bath (Fiebig et al., 2019).

We were not able to adequately standardize and report Δ_{49} data for this study, considering the number of replications per samples in combination with the low signal-to-noise ratio.

3. Results

3.1 XRD

Precipitated witherite sample DIC1 and samples heated in piston cylinder experiments were analyzed using X-ray powder diffraction to identify their mineralogy. Diffractograms were compared to those characteristic of the pure mineral phase (RRUFF database, see Lafuente et al., 2015; Supplementary File S3). All diffraction patterns corresponded to those expected for the respective pure minerals.

3.2 Clumped isotopes

Δ_{47} and Δ_{48} results for 8 calcitic samples reacted at both 90 and 110°C, are displayed in Table 3. Bulk ($\delta^{13}C_{VPDB}$, $\delta^{18}O_{VSMOW-CO2}$) and clumped ($\Delta_{47,\,CDES90}$ and $\Delta_{48,\,CDES90}$) isotopic compositions are presented for heated samples in Table 4 and for non-heated samples in Table 5. The entire dataset, replicate-level δ^{45}-δ^{49} values, as well as accompanying results, an overall sample summary and session-wise standardization parameters are accessible in Supplementary Tables S1 and S2, respectively.

Most heated samples were analyzed with 7-9 replicates, resulting in fully propagated 2SEs of ca. 7 ppm and 20 ppm for Δ_{47} and Δ_{48}, respectively (Table 4). Hence, we are able to confidently resolve differences of 10 ppm and 28 ppm in Δ_{47} and Δ_{48}, respectively, which is comparable to the ≤10 ppm, but significantly larger than the ≤1 ppm that are theoretically predicted for Δ_{63} and Δ_{64}, respectively, for aragonite, calcite and dolomite at temperatures ≥800°C (Schauble et al., 2006; Hill et al., 2014). Considering our analytical resolution of 10 ppm for Δ_{47}, we cannot resolve any temperature trend in the Δ_{47} data of re-ordered samples (Table 4). For a given mineralogy and acid digestion temperature, samples heated to temperatures of 800°C-1,200°C yield Δ_{47} and Δ_{48} values which are within their fully propagated 2SEs indistinguishable from each other. We are, therefore, confident that a stochastic distribution has been attained in all our heated samples.

Table 3: Clumped isotope ($\Delta_{47,\,CDES90}$, $\Delta_{47,\,CDES110}$, $\Delta_{48,\,CDES90}$ and $\Delta_{48,\,CDES110}$) values of samples reacted at 90 and 110°C, respectively. $\Delta^{*}_{i,\,110-90°C}$ corresponds to the difference between $\Delta_{i,\,CDES90}$ and $\Delta_{i,\,CDES110}$ values, 2SEs were determined through Gaussian error propagation of individual 2SEs for CDES90 and CDES110 (Supplementary Table S2).

Sample	N 90°C	N 110°C	$\Delta_{47,\,CDES90}$ (‰)	$\Delta_{47,\,CDES110}$ (‰)	$\Delta^{*}_{47,\,110-90°C}$ (‰)	2SE (‰)	$\Delta_{48,\,CDES90}$ (‰)	$\Delta_{48,\,CDES110}$ (‰)	$\Delta^{*}_{48,\,110-90°C}$ (‰)	2SE (‰)
Carrara	177	13	0.310	0.294	-0.0155	0.006	0.143	0.126	-0.0174	0.018
DHC2-8	23	7	0.570	0.557	-0.0133	0.008	0.233	0.224	-0.0087	0.026
ETH-1	637	26	0.207	0.194	-0.0126	0.005	0.127	0.122	-0.0050	0.014
ETH-1-1100	11	8	0.182	0.168	-0.0144	0.009	0.116	0.097	-0.0186	0.028
ETH-2	621	25	0.209	0.197	-0.0129	0.004	0.129	0.112	-0.0174	0.013
GU1	163	9	0.225	0.210	-0.0153	0.006	-0.399	-0.427	-0.0267	0.033
SA05	8	8	0.571	0.556	-0.0148	0.009	0.247	0.227	-0.0196	0.030
SA31	11	8	0.588	0.569	-0.0190	0.009	0.247	0.242	-0.0054	0.028
				weighted average (±2SE)	**-0.0147**	**0.002**			**-0.0148**	**0.006**

Table 4: $\delta^{13}C_{VPDB}$, $\delta^{18}O_{VSMOW-CO2}$, $\Delta_{47,\,CDES90}$ and $\Delta_{48,\,CDES90}$ values of aragonite, calcite, dolomite, siderite and witherite samples heated in piston cylinder experiments. *Values projected using mean $\Delta^{*}_{47,\,110-90°C}$ and $\Delta^{*}_{48,\,110-90°C}$ values of -0.0147±0.002 ‰ and -0.0148±0.006 ‰, respectively. ¶Gaussian error propagation of $\Delta^{*}_{i,\,110-90°C}$ 2SE of means (Table 3) and fully error propagated 2SE for Δ_i (Daëron, 2021). #Sample re-ordered at 850°C.

Sample	N	$\delta^{13}C_{VPDB}$ (‰)	$\delta^{18}O_{VSMOW-CO2}$ (‰)	$\Delta_{47,\,CDES90}$ (‰)	2SE (‰)	$\Delta_{48,\,CDES90}$ (‰)	2SE (‰)
Aragonite							
Arag1-800_72h	9	1.87	37.04	0.1877	0.0062	0.1202	0.0198
Arag2-800_48h	10	8.44	31.08	0.1819	0.0059	0.1126	0.0185
Bilin-1H#	9	3.09	31.01	0.1842	0.0061	0.1359	0.0189
Calcite							
ETH-1-1100	11	1.93	36.88	0.1824	0.0057	0.1157	0.0178
ETH-1-1100_110C	8	1.94	36.92	*0.1827	¶0.0073	*0.1119	¶0.0225
ETH-2-1100	19	-10.13	20.00	0.1826	0.0042	0.1218	0.0136
ETH1-800	10	1.93	36.96	0.1856	0.0059	0.1174	0.0188
ETH2-800_72h	10	-10.2	19.94	0.1863	0.0057	0.1358	0.0185
MERCK-800_48h	9	-42.1	23.07	0.1886	0.0064	0.1261	0.0193
Dolomite							
Dolo1_1200_110C	8	-0.66	32.75	*0.1799	¶0.0071	*0.1405	¶0.0221
Dolo2_800_110C	8	-0.47	33.18	*0.1770	¶0.0072	*0.1406	¶0.0221
Siderite							
Sid_800_64h_110C	8	-12.33	23.79	*0.1738	¶0.0070	*0.1274	¶0.0220
Witherite							
DIC1-1100_40h	7	-5.97	25.49	0.1808	0.0068	0.1096	0.0217
DIC1-800_72h	7	-6.00	25.12	0.1853	0.0068	0.1366	0.0217
DIC3-800_72h	9	-5.18	30.48	0.1847	0.0060	0.1101	0.0194

Table 5: $\delta^{13}C_{VPDB}$, $\delta^{18}O_{VSMOW-CO2}$, $\Delta_{47,\,CDES90}$ and $\Delta_{48,\,CDES90}$ results for aragonite, dolomite, witherite and siderite samples of un-/controlled lower formation temperature. *Values projected using mean $\Delta^{*}_{47,\,110-90°C}$ and $\Delta^{*}_{48,\,110-90°C}$ of -0.0147±0.002 ‰ and -0.0148±0.006 ‰, respectively. ¶Gaussian error propagation of $\Delta^{*}_{i,\,110-90°C}$ 2SE of means (Table 3) and fully error propagated 2SE for Δ_i (Daëron, 2021). †Considered proto-dolomite.

Sample	N	$\delta^{13}C_{VPDB}$ (‰)	$\delta^{18}O_{VSMOW-CO2}$ (‰)	$\Delta_{47,\,CDES90}$ (‰)	2SE (‰)	$\Delta_{48,\,CDES90}$ (‰)	2SE (‰)
Aragonite							
AI_006	7	0.05	41.79	0.632	0.007	0.271	0.023
RM1	9	1.49	41.12	0.646	0.007	0.255	0.022
RM1 (110°C)	9	1.61	41.16	*0.634	¶0.007	*0.250	¶0.021
Dolomite							
D-Mio-1798	6	2.40	34.80	*0.529	¶0.009	*0.207	¶0.027
D-Mio-3010	6	4.24	33.25	*0.526	¶0.009	*0.190	¶0.027
D-Mio-3016	6	4.32	33.43	*0.521	¶0.009	*0.223	¶0.028
D-Mio-3056	6	5.16	34.12	*0.540	¶0.009	*0.247	¶0.028
D-Mio-474	6	3.40	33.19	*0.540	¶0.009	*0.219	¶0.027
D-Mio-5520	6	8.14	36.68	*0.552	¶0.010	*0.207	¶0.027
Dolomite_350A-9	7	-55.72	7.06	*0.246	¶0.008	*0.148	¶0.024
Dolomite_80-1†	8	-6.74	23.95	*0.468	¶0.007	*0.331	¶0.023
Dolomite_BE	9	-10.02	44.07	*0.593	¶0.007	*0.252	¶0.022
IPGP-SRM88-1	8	2.20	32.87	*0.502	¶0.007	*0.206	¶0.022
IPGP-INYO	9	-0.61	32.90	*0.236	¶0.007	*0.136	¶0.021
Siderite							
IPGP-SID1	8	-12.20	23.86	*0.307	¶0.007	*0.165	¶0.022
Sid_D1	10	14.11	34.37	*0.559	¶0.007	*0.238	¶0.020
Sid_D2	10	17.23	36.54	*0.590	¶0.007	*0.244	¶0.021
Sid_D3	10	18.58	37.21	*0.588	¶0.007	*0.251	¶0.021
Sid_D4	9	18.51	37.12	*0.592	¶0.007	*0.244	¶0.021
Sid_D5	9	15.42	35.31	*0.568	¶0.007	*0.238	¶0.021
Sid_D6	10	-10.53	31.76	*0.511	¶0.006	*0.219	¶0.020
Witherite							
DIC1	6	-5.86	26.18	0.590	0.007	0.260	0.023

3.3 Determination of the difference in acid fractionation factors between 90 and 110°C reactions

In order to quantify the effect of acid digestion temperature on measured Δ_{47} and Δ_{48} values, we analyzed a suite of calcites at both 90 and 110°C. This enables determining differences in $\Delta_{i,\,CDES110} - \Delta_{i,\,CDES90}$ values, expressed as $\Delta^*_{i,\,110-90°C}$. Guo et al. (2009) predicted a weak temperature dependence of 0.035‰ in $\Delta^*_{47,\,25°C}$ for every 1‰ increase in Δ_{63}, due to the circumstance that ^{17}O-bearing isotopologues contribute slightly, but in different proportions to overall masses 63 and 47. On the contrary, the contribution of ^{17}O-bearing isotopologues to overall masses 64 and 48 is negligibly small, such that Δ_{64} is not expected to affect Δ^*_{48} significantly at any digestion temperature. In any case, compositional effects occurring at acid digestion temperatures of 90°C and 110°C should cancel each other out if the difference in acid fractionation factors $\Delta^*_{i,\,110-90°C}$ is addressed. As expected, no significant slope is found for correlations between $\Delta^*_{47,\,110-90°C}$ and $\Delta_{47,\,CDES90}$ (as a measure of Δ_{63}) and between $\Delta^*_{48,\,110-90°C}$ *and* $\Delta_{48,\,CDES90}$ (as a measure of Δ_{64}) (see Figures 4 and 5). Throughout the following, we use average $\Delta^*_{47,\,110-90°C}$ and $\Delta^*_{48,\,110-90°C}$ values of -0.0147 ‰ and -0.0148 ‰, respectively, to project CDES110 data to the CDES90. We further assume that these calcite-specific $\Delta^*_{i,\,110-90°C}$ are also valid for dolomite and siderite.

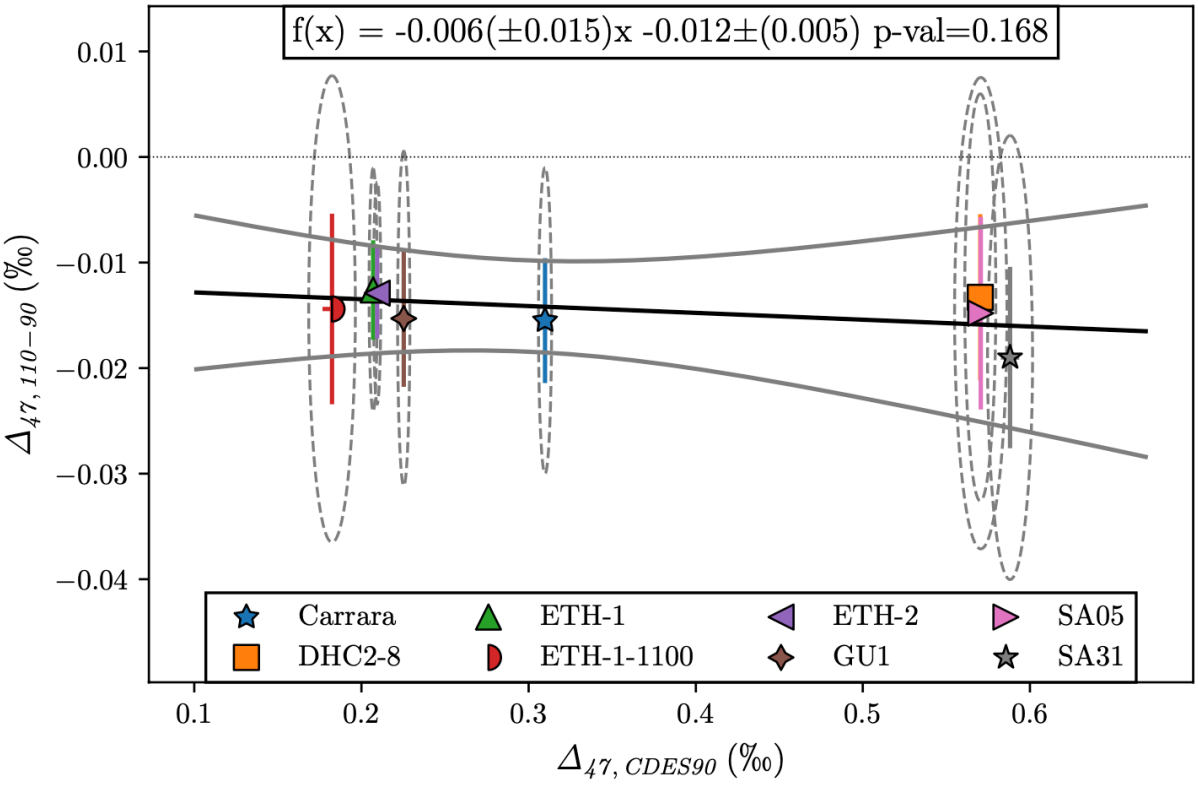

Figure 4: Differences between $\Delta_{47,\,CDES90}$ and $\Delta_{47,\,CDES110}$ (i.e., $\Delta^*_{47,\,110-90°C}$) as a function of $\Delta_{47,\,CDES90}$ for several calcite samples. No significant correlation is observed, as demonstrated through p-value >0.05 when using OGLS regression (Daëron & Vermeesch, 2024).

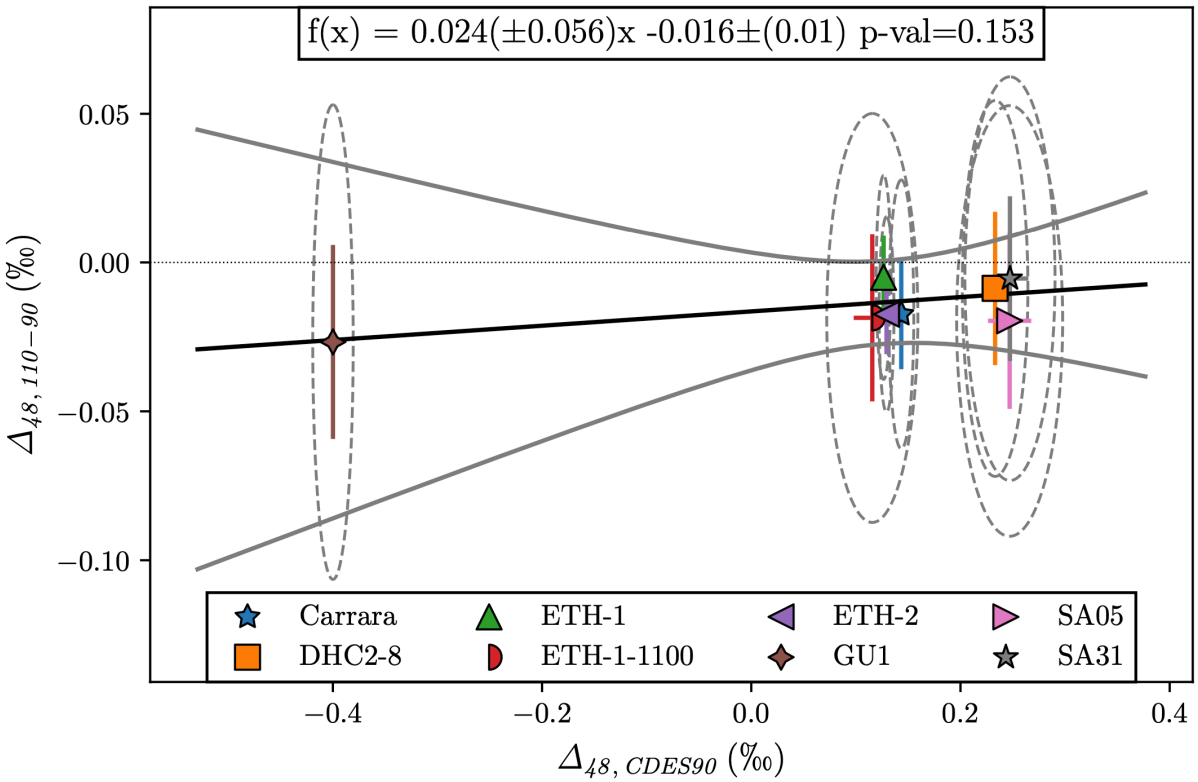

Figure 5: Differences between $\Delta_{48,\,CDES90}$ and $\Delta_{48,\,CDES110}$ (i.e., $\Delta^{*}_{48,\,110-90°C}$) as a function of $\Delta_{47,\,CDES90}$ for several calcite samples. No significant correlation is observed, as demonstrated through p-value >0.05 when using OGLS regression (Daëron & Vermeesch, 2024).

4. Discussion

4.1 Acid fractionation factors derived from samples heated to stochastic composition

According to the theoretical model of Guo et al. (2009), differences of up to 30 ppm in Δ^{*}_{47} for aragonite, calcite, witherite and dolomite were predicted. Δ^{*}_{47} has been determined experimentally by Guo et al. (2009), who melted three calcitic samples, reacted these directly at 25°C and obtained an average Δ^{*}_{47} of 0.232±0.015 ‰ (1SD) on the internal Caltech scale. Later, following the introduction of the absolute reference frame (ARF) by Dennis et al., (2011), Passey & Henkes (2012) heated calcite to a temperature of 800°C and reacted this sample at 90°C. Their resulting $\Delta^{*}_{47,\,\mathrm{CDES90}}$ value of 0.213 ‰ corresponded to a $\Delta^{*}_{47,\,\mathrm{CDES25}}$ value of 0.294 ‰, considering the $\Delta^{*}_{47,\,90-25°C}$ of -0.081 ‰ of Passey et al. (2010). This $\Delta^{*}_{47,\,\mathrm{CDES25}}$ value agreed with the $\Delta^{*}_{47,\,\mathrm{CDES25}}$ value of 0.280±0.016 ‰ (error represents replicate-based 1SD) reported by Tripati et al. (2015), who reprocessed the data of Guo et al. (2009) using heated gases and NBS 19 as anchors for ARF projection (Dennis et al., 2011). For a melted witherite sample, Tripati et al. (2015) reported a $\Delta^{*}_{47,\,\mathrm{CDES90}}$ value of 0.163±0.006 ‰ (error represents replicate-based 1SD), which was projected into the CDES25 using $\Delta^{*}_{47,\,90-25°C}$ of -0.092 ‰ (Henkes et al., 2013), finally yielding a $\Delta^{*}_{47,\,\mathrm{CDES25}}$ value of 0.255±0.006 ‰ (1SD), i.e., significantly lower than the one reprocessed for calcite. A more comprehensive study of Müller et al. (2017) investigated the Δ^{*}_{47} values of aragonite, calcite and dolomite which were heated to temperatures ≥850°C. They reacted samples both at 70°C

using the Kiel IV setup and offline in McCrea type reaction vessels at 100°C. The CO_2 released at 70°C was introduced into the mass spectrometer using the micro volume mode of the Kiel IV, whereas the dual inlet was used for the CO_2 extracted at 100°C. They obtained significantly distinct AFFs for 70°C reactions of aragonite ($\Delta^*_{47,\,\mathrm{CDES70}}$ = 0.172±0.003), calcite ($\Delta^*_{47,\,\mathrm{CDES70}}$ = 0.197±0.002) and dolomite ($\Delta^*_{47,\,\mathrm{CDES70}}$ = 0.226±0.002, errors representing non-propagated, replicate-based 1SE). Their study, therefore, confirmed that calcite and dolomite may exhibit different Δ^*_{47}-T_{acid} relationships, as originally postulated by Murray et al. (2016).

Bonifacie et al. (2017) indirectly estimated that the AFF at 90°C for dolomite was $\Delta^*_{47,\,CDES90}$ = 0.176 ‰, by comparing their $\Delta_{47,\,CDES90}$-T calibration regression line based on dolomites covering a large range of formation temperatures (between 25 and 350°C) with the theoretically determined Δ_{63}-T relationship for dolomite (Schauble et al., 2006). As expressed by these authors, this value was slightly lower than the $\Delta^*_{47,\,CDES90}$ value of 0.198 ± 0.008 ‰ obtained from the intercept of the $\Delta_{47,\,CDES25}$-T relationship by Passey & Henkes (2012) corrected for their experimentally determined $\Delta^*_{47,\,90-25°C}$, but matched the internal Caltech scale $\Delta^*_{47,\,25°C}$ value of melted calcites from Guo et al. (2009) after projecting this value into the CDES90 using the Caltech-specific tertiary transfer function of Dennis et al. (2011). Based on this observation and their additional finding that $\Delta_{47,\,CDES90}$ values obtained on calcite and dolomite were comparable, Bonifacie et al (2017) proposed that calcite and dolomite exhibit not only similar $\Delta^*_{47,\,CDES90}$, but also comparable $\Delta_{47,\,CDES90}$-T relationships.

All analytical measurements for the aforementioned studies were produced using the first generation of gas source mass spectrometers. Accuracy and precision of corresponding measurements were likely affected by non-optimal correction for the negative PBL effect (Fiebig et al., 2016). In addition, non-unique temperature dependencies of AFFs were considered for the comparison of Δ_{47} values obtained at different reaction temperatures (Petersen et al., 2019). Ultimately, non-optimal ^{17}O correction parameters (Daëron et al., 2016; Petersen et al., 2019; Schauer et al., 2016) were used in some of these studies, and full error propagation (Daëron, 2021) was not considered. Recently, Fiebig et al. (2021) reacted two calcites heated at 1,100°C in a CAB and obtained $\Delta^*_{47,\,CDES90}$ values of 0.179±0.006 ‰ and 0.184±0.006 ‰ (fully error propagated 2SE). Anderson et al. (2024) reacted dolomites which were re-ordered at 1,100-1,200°C, at an acid digestion temperature of 70°C. They projected mass spectrometric raw data to a reaction temperature of 90°C using calcite anchors ETH-1, ETH-2, ETH-3, ETH-4 and IAEA-C2 (Bernasconi et al., 2021), finally obtaining $\Delta^*_{47,I-CDES}$ values ranging from 0.180 to 0.184 ‰ (Anderson et al., 2024). Note that I-CDES values should perfectly align with CDES90 values since the former scale has been anchored relative to the latter. Furthermore, these values agreed perfectly with the calcite-specific $\Delta^*_{47,\,CDES90}$ values of Fiebig et al. (2021), suggesting that calcite and dolomite have indistinguishable Δ^*_{47} for a given acid reaction temperature in the range of 70-90°C. Latest I-CDES results of Kong et al. (2023) implied that AFFs for witherite and calcite are identical as well. These authors reacted witherite reordered at 600°C at an acid digestion temperature of 90°C, obtaining a $\Delta_{47,I-CDES}$ value of 0.213±0.021 ‰. This value is indistinguishable from the

$\Delta_{47,I-CDES}$ values of 0.2052±0.0016 ‰ and 0.2085±0.0015 ‰ assigned to ETH-1 and ETH-2, respectively, which represent calcites that were also equilibrated at 600°C (Bernasconi et al., 2021).

To make our clumped isotope data generated at the two distinct temperatures of 110°C and 90°C comparable, we projected all CDES110 data into the CDES90 using our calcite-specific $\Delta^*_{47,\,110-90°C}$ and $\Delta^*_{48,\,110-90°C}$ values (Table 4, Section 3.3 , Figure 6). Doing so, we inherently assume that calcite-specific $\Delta^*_{47,\,110-90°C}$ and $\Delta^*_{48,\,110-90°C}$ are also valid for all other investigated mineralogies. Considering the limited sample sizes (i.e., number of replicates) of each individual group of stochastic samples (n between 1 and 6 across five groups), classic parametric tests, such as ANOVA and t-tests are not applicable to identify significant differences in $\Delta^*_{47,\,CDES90}$ and $\Delta^*_{48,\,CDES90}$ values between groups. Instead, we employed non-parametric tests which do not rely on distributional assumptions and are more robust in this context (Zimmerman, 2000). We used the Kruskal-Wallis H-test for overall group comparisons, as it can handle groups of different sizes and does not assume normality (Kruskal & Wallis, 1952). Additionally, for pairwise comparisons, we utilized Mann-Whitney U tests, which are suitable for small, unequal sample sizes (Mann & Whitney, 1947). Both the Kruskal-Wallis H-test (H=7.17, p=0.127 and H=5.81, p=0.214, respectively) and the pairwise Mann-Whitney U tests (all corr. p≥0.71) revealed no significant difference in $\Delta^*_{47,\,CDES90}$ and $\Delta^*_{48,\,CDES90}$ values between stochastic calcite, aragonite, dolomite, witherite and siderite. Only one thermally reset siderite sample was measured, therefore, we cannot guarantee that its corresponding $\Delta^*_{47,\,CDES90}$ and $\Delta^*_{48,\,CDES90}$ values are perfectly representative. However, Holme et al. (2023) reacted siderite and calcite at 90°C using a CAB. Three replicates of a siderite equilibrated at 625°C yielded a mean $\Delta_{47,\,CDES90}$ value of 0.206±0.006 ‰ (1 SE). This value is in excellent agreement with $\Delta_{47,\,CDES90}$ values obtained for InterCarb calcite anchors ETH-1 (0.2052±0.0016 ‰) and ETH-2 (0.2085±0.0015 ‰; 1SEs), both of which were heated to 600°C (Bernasconi et al. 2021). Their results, therefore, seem to confirm that calcite and siderite have indistinguishable $\Delta^*_{47,\,CDES90}$.

We conclude that there is no indication for significant differences in Δ^*_{47} and Δ^*_{48} values between calcite, aragonite, dolomite, witherite and siderite at a given temperature in the range 90-110°C. The overall error-weighted average $\Delta^*_{47,\,CDES90}$ value is 0.1850±0.0042 ‰ and the $\Delta^*_{48,\,CDES90}$ value is 0.1255±0.0130 ‰, both in excellent agreement with recently published estimations of calibration intercepts of 0.1848 ‰ and 0.1214 ‰ obtained for calcite (Fiebig et al., 2024).

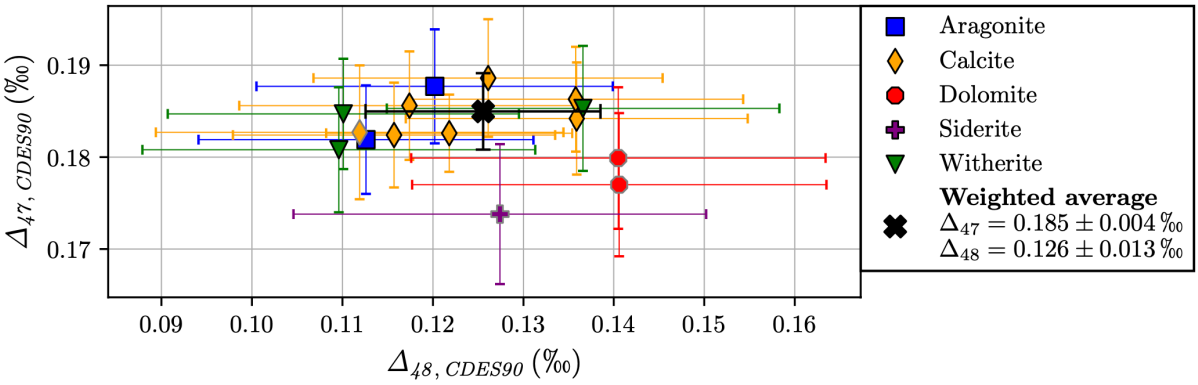

Figure 6: Dual clumped isotope ($\Delta_{47,\ CDES90}$ and $\Delta_{48,\ CDES90}$) results (±2SE) for investigated stochastic samples of different mineralogies. CDES110 data (grey outlined markers) was projected into the CDES90 using calcite-derived $\Delta^*_{47,\ 110\text{–}90°C}$ and $\Delta^*_{48,\ 110\text{–}90°C}$ values of -0.0147 and -0.0148 ‰, respectively (Table 3). See text for further information.

4.2 Non-stochastic samples of lower formation temperatures

The $\Delta_{47,\ CDES90}$ and $\Delta_{48,\ CDES90}$ compositions of non-stochastic samples formed at known and unknown temperatures are shown relative to the calcite equilibrium line (Fiebig et al., 2024) in Figures 7 and 8, respectively. This information, paired with our observations on acid fractionation factors (Section 4.1), can resolve if there is any significant difference in Δ_{63}-Δ_{64}-T relationships between these minerals.

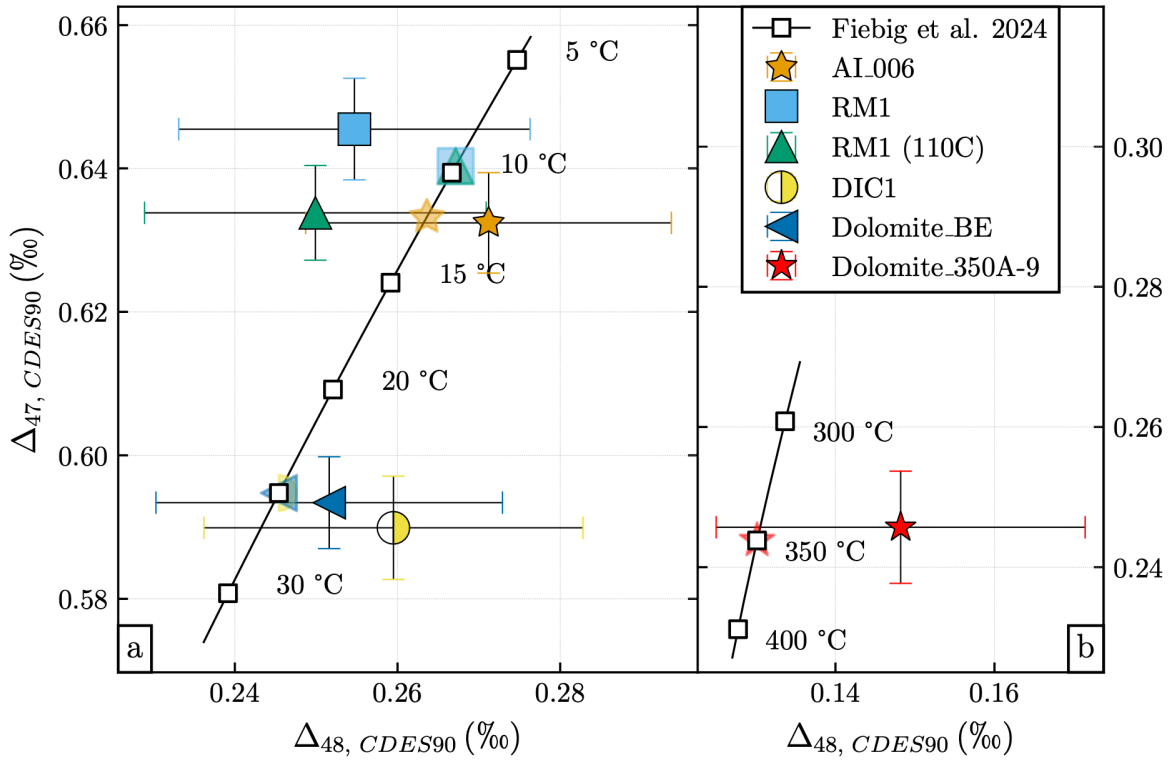

Figure 7: Dual clumped isotope composition ($\Delta_{47,\ CDES90}$ and $\Delta_{48,\ CDES90}$) of non-stochastic samples of known lower formation temperatures, displayed relative to the calcite-specific temperature equilibrium relationship (Fiebig et al., 2024). Aragonite sample RM1 (110C) and dolomite samples have been acid digested at 110°C and projected into the CDES90 using calcite-derived $\Delta^*_{47,\ 110\text{–}90°C}$ and $\Delta^*_{48,\ 110\text{–}90°C}$ values of -0.0147 ‰ and -0.0148 ‰, respectively (Table 3). Transparent markers on the Δ_{47}-Δ_{48} temperature equilibrium line indicate known formation temperatures.

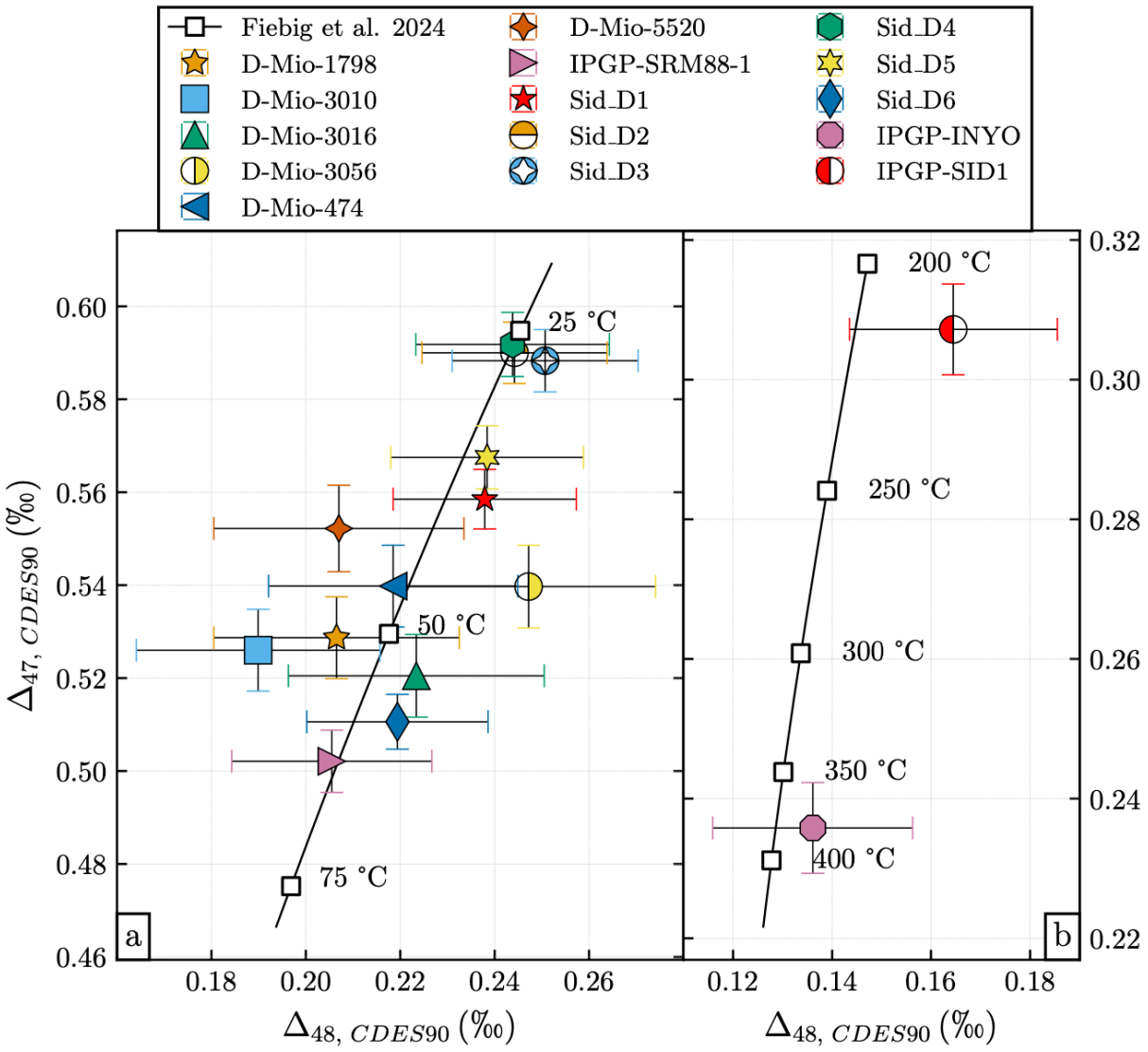

Figure 8: Dual clumped isotope composition ($\Delta_{47,\,CDES90}$ and $\Delta_{48,\,CDES90}$) of non-stochastic samples of unknown lower formation temperatures, displayed relative to the calcite-specific temperature equilibrium relationship (Fiebig et al., 2024). Samples have been acid digested at 110°C and projected into the CDES90 using calcite-derived $\Delta^*_{47,\,110\text{–}90°C}$ and $\Delta^*_{48,\,110\text{–}90°C}$ values of -0.0147 ‰ and -0.0148 ‰, respectively (Table 3).

4.2.1 Aragonite

Early studies on aragonite assumed that the temperature dependences of aragonite- and calcite-Δ_{47} are indistinguishable, thus applying calcite-based calibrations to determine aragonite formation temperature (e.g., Came et al., 2007). Validity of this assumption was confirmed in numerous independent investigations. Tripati et al. (2010), presenting a Δ_{47}-T calibration on aragonitic and calcitic foraminifera and coccoliths, and Henkes et al. (2013), providing a Δ_{47}-T calibration largely based on aragonitic and calcitic mollusks, did not resolve any significant differences between aragonite and calcite. The first pure synthetic aragonite Δ_{47}-T calibration (Defliese et al., 2015) was indistinguishable from a calcite calibration produced by the same authors, and also from the calcite calibration of Wacker et al. (2014). Kele et al. (2015) reacted aragonite and calcite at 70°C using the Kiel IV analytical setup and showed that both have very similar Δ_{47}-T relationships. Kelson et al. (2017) precipitated

calcite and aragonite samples at identical temperatures, reacted at both 25°C and 90°C and likewise found indistinguishable Δ_{47}-T relationships. In a recent, comprehensive study (70°C acid digestion using a Kiel IV, ETH anchor standardization to I-CDES), biogenic (1-18°C) and abiogenic (1-850°C) aragonite samples of controlled formation temperature were analyzed (de Winter et al., 2022). No significant offsets were displayed relative to the unified calibration of Anderson et al. (2021) which is largely based on calcite. So far, studies applying dual clumped isotopes to aragonite have directly applied calcite-specific calibrations to identify kinetic biases and/or infer carbonate formation temperatures (Arndt et al., 2025; Bajnai et al., 2020; Davies et al., 2022; Fiebig et al., 2021; Kniest et al., 2024; Lu et al., 2024; Parvez et al., 2023; Staudigel et al., 2024).

Our $\Delta_{47,\,CDES90}$ and $\Delta_{48,\,CDES90}$ values for biogenic aragonite samples **AI_006** and **RM1** plot indistinguishably from calcite equilibrium (Figure 7). $\Delta_{47,\,CDES90}$-derived temperatures of $12.3^{+2.3}_{-2.3}$°C (**AI_006**) and $8.1^{+2.3}_{-2.3}$°C (**RM1**) agree within ±2SEs with their formation temperatures of 12.0°C and $9.7^{+4.3}_{-3.7}$°C, respectively. Sample **RM1** was additionally reacted at 110°C (**RM1 (110C)**). Applying calcite-derived $\Delta^{*}_{47,\,110\text{–}90°C}$ and $\Delta^{*}_{48,\,110\text{–}90°C}$ of -0.0147 ‰ and -0.0148 ‰, respectively, to its measured $\Delta_{i,\,CDES110}$ values finally yields $\Delta_{i,\,CDES90}$ values which are within 2SEs indistinguishable from those obtained on **RM1**. The $\Delta_{47,\,CDES90}$-derived temperature of $11.8^{+2.2}_{-2.1}$°C is again consistent with the known formation temperature (Figure 7, Table 5).

Our high-precision results, therefore, confirm previous evidence that aragonite and calcite follow a single Δ_{47}-T equilibrium relationship. Differences in Δ_{48} are below analytical resolution as well. Considering these indistinguishable AFFs between calcite and aragonite (Section 4.1), we propose that samples of aragonite follow the same Δ_{63}-T and Δ_{64}-T relationships as calcite. Conclusively, the equilibrium Δ_{47}-Δ_{48}-T calibrations of Fiebig et al. (2021; 2024) and Swart et al. (2021), which are indistinguishable from each other within errors, can also be applied to aragonite.

4.2.2 Dolomite

Winkelstern et al. (2016) reacted natural and synthetic dolomites of known formation temperatures (20-250°C) at an acid digestion temperature of 75°C. In the low temperature range, their $\Delta_{47,\,CDES25}$-T calibration was indistinguishable from those of Defliese et al. (2015) for calcite and aragonite precipitated at 5-70°C. A single Δ_{47}-T relationship for calcite and dolomite was also proposed by Bonifacie et al. (2017), who reacted at 90°C natural and synthetic samples of controlled formation temperatures (25-350°C). Conversely, differences between calcite and dolomite were reported by Müller et al. (2019). They reacted dolomites of controlled formation temperatures at 70°C and compared the dolomite $\Delta_{47,\,CDES70}$-T relationship to the calcite/aragonite $\Delta_{47,\,CDES70}$-T relationship of Kele et al. (2015), produced in the same laboratory and recalculated after Bernasconi et al. (2018). They determined that, for a given temperature, dolomite-$\Delta_{47,\,CDES70}$ exceeded calcite-$\Delta_{47,\,CDES70}$ by ~30 ppm, a value that exactly corresponded to the difference in $\Delta^{*}_{47,\,CDES70}$ between dolomite and calcite

observed by Müller et al. (2017). Their findings of inconsistent behavior between dolomite and calcite were confirmed by Fosu et al. (2023), who modified the Kiel IV device to perform 90°C acid reactions. These authors, again, obtained significantly different calcite and dolomite $\Delta_{47,\,I-CDES}$-T relationships. In the most recent study of Anderson et al. (2024), dolomite samples of controlled formation temperatures (25-1,200°C) were reacted at 70°C. As in the study of Fosu et al. (2023), mass spectrometric raw data was corrected using IUPAC parameters and calcite-based I-CDES standardization (Bernasconi et al., 2021). The corresponding $\Delta_{47,\,I-CDES}$-T relationship was indistinguishable from that of calcite after Anderson et al. (2021) who reacted calcites at the same temperature and processed data the same way as described in Anderson et al. (2024). Indirect evidence for calcite-like behavior of dolomites is further given through a dual clumped isotope study focusing on paired calcite and dolomite samples in an alteration setting (Lu et al., 2023).

Our dataset confirms previous studies that postulated the validity of a single Δ_{47}-T relationship for both calcite and dolomite. Two dolomite calibration samples of Bonifacie et al. (2017) are characterized by clumped isotope compositions that are indistinguishable within their 2SEs from the calcite equilibrium relationship (Fiebig et al., 2024) (Figures 7a, b). Moreover, $\Delta_{47,\,CDES90}$ values of 0.246±0.008 ‰ (**Dolomite_350A-9**) and 0.593±0.006 ‰ (**Dolomite_BE**), projected to the calcite equilibrium Δ_{47}-T relationship of Fiebig et al. (2024), reflect temperatures of 344^{+29}_{-25}°C and $25.5^{+2.3}_{-2.2}$°C, perfectly matching known formation temperatures of 351.4±2°C and 25±4°C. On the contrary, sample **Dolomite_80-1**, which has been precipitated through mixing of $MgSO_4$, $Ca(NO_3)_2$*$4H_2O$, and Na_2CO_3 solutions at 80.2±1°C, deviates significantly from the calcite equilibrium line. It exhibits a relatively large $+\Delta_{48}$ bias relative to its predicted equilibrium composition (Figure 9). It has been shown by Hu et al. (2019), that nitrate, if present along with the carbonate, decomposes to NO_2 during phosphoric acid digestion. Nitrate-derived NO_2 is not successfully removed from analyte CO_2 through gas purification, ultimately acting as isobaric interferent, thereby compromising Δ_{47} and Δ_{48} values (Fiebig et al., 2024). Notably, the slope displayed by replicate Δ_{47}/Δ_{48} data of **Dolomite_80-1** agrees within errors with the theoretical slope of -0.3±0.05 indicative of NO_2 contamination (Figure 9). We therefore propose that this sample has been precipitated under disequilibrium conditions and that its $\Delta_{47,\,CDES90}$ value fortuitously corresponded to a temperature of 80°C when analyzed by Bonifacie et al. (2017). Notably, our $\Delta_{47,\,CDES90}$ value of 0.468±0.007 ‰ (fully propagated 2SE) obtained for this sample is identical to the 0.469±0.009 ‰ (non-propagated, replicate-based 2SE) reported by Bonifacie et al. (2017), implying that the degree of NO_2^+ contamination was comparable in the two analytical setups used at GU and IPGP.

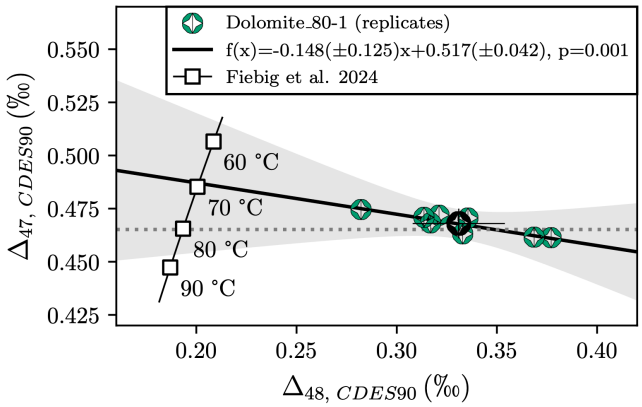

Figure 9: Individual replicate $\Delta_{47,\,CDES90}$ and $\Delta_{48,\,CDES90}$ values (projected utilizing $\Delta^*_{47,\,110\text{–}90°C}$ and $\Delta^*_{48,\,110\text{–}90°C}$ values of -0.0147 and -0.0148 ‰, respectively, see Table 3) for sample Dolomite_80-1 show significant correlation (p=0.001), sample mean value ±2SEs displayed with black marker. The slope agrees within errors to that predicted for isobaric contamination through NO_2 (Fiebig et al., 2024). Back-extrapolating this vector intersects the equilibrium at a temperature of ca. 70°C, which is 10°C colder than the precipitation temperature of ca. 80°C (dotted horizontal line).

Dolomite samples of unknown formation temperatures (**D-Mio**, **IPGP-SRM88-1** and **IPGP-INYO**, Table 3) also plot indistinguishable from calcite Δ_{47}/Δ_{48} equilibrium (Figures 8a, b). Measured $\Delta_{47,\,CDES90}$ values for samples **D-Mio** reflect reasonable temperatures within the range 37-58°C, which are in accordance with the maximal temperature estimate of 60°C obtained through vitrinite reflectance measurements. The same applies to samples **IPGP-SRM88-1** and **IPGP-INYO** whose $\Delta_{47,\,CDES90}$ values indicate formation temperatures of $62.0^{+3.3}_{-3.1}$°C and $380^{+30.1}_{-25.8}$°C, respectively.

Taking into account that calcite and dolomite exhibit indistinguishable AFFs (Section 4.1), we suggest that calcite and dolomite also share Δ_{63}-T and Δ_{64}-T relationships. Accordingly, the equilibrium Δ_{47}-Δ_{48}-1/T calibrations characteristic of calcite (Fiebig et al., 2021; 2024; Swart et al., 2021) can be applied to dolomite as well.

4.2.3 Witherite

There are several studies in which witherite was precipitated under controlled temperature conditions for clumped isotope analysis (e.g., Kong et al., 2023, Staudigel & Swart, 2018, Uchikawa et al., 2021). However, it should be noted that these publications precipitated the dissolved inorganic carbon (DIC) pool quantitatively, so that corresponding Δ_{47} values reflect DIC composition rather than witherite precipitated under equilibrium conditions. This most likely is the reason why e.g., the precipitates of Kong et al. (2023) have an average +15 ppm difference when compared to the calcite Δ_{47}-T relationship of Fiebig et al. (2024). Our low-temperature witherite sample, **DIC1**, which was precipitated from isotopically equilibrated solutions (5 % removal of DIC during precipitation), plots indistinguishably from dual clumped isotope equilibrium (Figure 7a). Its measured $\Delta_{47,\,CDES90}$ of 0.590±0.007‰, projected to the calcite equilibrium Δ_{47}-T relationship of Fiebig et al. (2024), yields a temperature of $26.7^{+2.6}_{-2.6}$°C that exactly confirms its known formation temperature of 25°C. This finding, along with our measured indistinguishable Δ^*_{47} and Δ^*_{48} AFFs for calcite and witherite (Section 4.1) strongly

implies that calcite and witherite share the same Δ_{47}-T and Δ_{48}-T equilibrium relationships over the entire temperature range from 25-1100°C. Because differences in Δ^*_{47}, Δ^*_{48}, Δ_{47}-T and Δ_{48}-T between calcite and witherite are insignificant, it follows that Δ_{63}-T and Δ_{64}-T relationships are also identical.

4.2.4 Siderite

Fernandez et al. (2014) reacted siderite and calcite formed at known temperatures at 100°C and could not resolve any significant differences in corresponding Δ_{47}-T relationships. In the most recent study of Holme et al. (2023), siderite was reacted at 90°C. These authors observed that their apparent Δ_{47}-T relationship for pure siderite departed by -20 ppm from the composite Δ_{47}-T calcite calibration of Petersen et al. (2019) which considered synthetically precipitated calcite (Defliese et al., 2015; Kelson et al., 2017; Kluge et al., 2015; Passey & Henkes, 2012; Tang et al., 2014), aragonite (Defliese et al., 2015; Kelson et al., 2017; Kluge et al., 2015), dolomite (Winkelstern et al., 2016), and siderite (Fernandez et al., 2014). For a given temperature, Petersen et al. (2019) did not find any significant differences in Δ_{47} values between all these mineralogies when all original data was reprocessed using IUPAC parameters. A systematic offset to lower Δ_{47} values, however, was also observed by van Dijk et al. (2019) when comparing their siderite-$\Delta_{47,\,CDES70}$ values to those obtained on calcite and aragonite presented by Kele et al. (2015). Van Dijk et al. (2019) attributed the observed discrepancy to differences in the acid fractionation factor between siderite and aragonite/calcite. This interpretation was not supported by the data of Holme et al. (2023), who explained the observed offset of siderite Δ_{47} with respect to calcite with supersaturation-related kinetic isotope effects being recorded in siderite.

After correction for calcite-specific $\Delta^*_{47,\,110-90°C}$ and $\Delta^*_{48,\,110-90°C}$ values, $\Delta_{47,\,CDES90}$ and $\Delta_{48,\,CDES90}$ values of CO_2 extracted from our natural siderite samples **Sid_D1-Sid_D6** at 110°C (Section 3.3) are within error, indistinguishable from the proposed calcite equilibrium relationship (Fiebig et al., 2024) (Figure 8a). The dual clumped isotope composition of IPGPs internal siderite standard, **IPGP-SID1**, also falls on the calcite equilibrium line (Figure 8b). Its $\Delta_{47,\,CDES90}$-derived temperature is 213^{+10}_{-9} °C. At a first glance, these results, therefore, do support previous findings according to which siderite and calcite are characterized by identical equilibrium Δ_{47}-T relationships (e.g., Fernandez et al., 2014; Petersen et al., 2019). However, in our case, formation temperatures and conditions (e.g., precipitation rates) of investigated siderites are unknown. We, therefore, cannot rule out that their dual clumped compositions were biased by kinetics and only fortuitously correspond to equilibrium. In any case, more analyses on siderites precipitated under controlled conditions, devoid of kinetic bias, are necessary to evaluate with more confidence if siderite and calcite are characterized by a common Δ_{47}-Δ_{48}-T relationship.

5. Conclusions

We have investigated the dual clumped isotope compositions of stochastic and low-temperature samples of calcite, aragonite, dolomite, witherite and siderite at acid digestion temperatures of 90 and 110°C. Data projected to the CDES90 shows no significant differences in acid fractionation factors between investigated mineralogies. $\Delta_{47,\,\mathrm{CDES90}}$ values of low-temperature samples of aragonite, dolomite, witherite and siderite plot indistinguishably from the equilibrium calcite Δ_{47}-Δ_{48}-T relationship of Fiebig et al. (2021) revised after Fiebig et al. (2024), and $\Delta_{47,\,CDES90}$ values of aragonite, dolomite and witherite samples exactly confirm known formation temperatures. These results demonstrate that a single Δ_{47}-Δ_{48}-T relationship is valid for calcite, aragonite, dolomite and witherite. We do not have any indication that this relationship might not be applicable to siderite, however high-precision data on siderites precipitated under controlled conditions is necessary to confirm this hypothesis. The universal application of calcite-specific Δ_{47}-Δ_{48}-T relationships to aragonite, dolomite and witherite provides a promising framework for consistent isotopic analyses in different carbonate samples. These results have significant implications for improving the accuracy of temperature reconstructions in paleoenvironmental studies.

Acknowledgements

J.F. acknowledges funding through DFG, Reinhart Koselleck project FI-948/13-1 and E.H. acknowledges DFG funding HA-5137/5. Sven Hofmann is acknowledged for technical support. We would like to thank Vanessa Schlidt, Amelia Davies, Mattia Tagliavento, Manuel Schumann, Phil Dolz and Armelle Ballian for assistance in the clumped isotope laboratory. We thank Niels de Winter and Vanessa Schlidt for providing samples AI_006 and RM1, respectively. Juske Horita is acknowledged for providing (proto)dolomites. We acknowledge Karel Mach, Chief Geologist at the Bilina Mine, for providing siderite material.

CRediT statement

Bernecker Miguel: Methodology, Software, Validation, Formal analysis, Investigation, Data Curation, Writing - Original Draft, Writing - Review & Editing, Visualization, Supervision, Project administration, Funding acquisition. **Bonifacie Magali**: Conceptualization, Methodology, Resources, Writing - Review & Editing, Project administration. **Staudigel Philip**: Investigation, Writing - Review & Editing. **Meijer Niels**: Investigation, Writing - Review & Editing. **Siebert Julien**: Investigation. **Wehr Nicolas**: Investigation. **Haussühl Eiken**: Investigation, Writing - Review & Editing, Funding acquisition. **Bernasconi Stefano M.**: Resources, Writing - Review & Editing. **Petrash Daniel**: Resources, Writing - Review & Editing. **Dietzel Martin**: Resources. **Fiebig Jens**: Conceptualization, Methodology, Investigation, Writing - Original Draft, Writing - Review & Editing, Supervision, Project administration, Funding acquisition.

Appendix A. Supplementary Material

Clumped isotope data utilized for this manuscript can be found in Supplementary Materials S1 and S2 (spreadsheets). Supplementary Materials S1 keeps the mass-spectrometric input data as pre-processed δ^{45}-δ^{49} values, which were determined from baseline-corrected raw data. Clumped isotope processing result containing replicate-level results, a sample overview summary, as well as session-wise standardization parameters and statistics are stored in Supplementary Material S2. X-ray diffractograms for our thermally re-ordered samples and DIC1 (Section 3.1) are available from Supplementary Material S3 (document).

Data Availability

Research data are available from https://doi.org/10.5281/zenodo.14843259, and from the Supplementary Materials S1 and S2.

References

Anderson, N. T., Bonifacie, M., Jost, A. B., Siebert, J., Bontognali, T., Horita, J., Müller, I. A., Bernasconi, S. M., & Bergmann, K. D. (2024). Re-Assessing the Need for Apatite- and Dolomite-Specific Calibrations of the Carbonate Clumped Isotope Thermometer. *Geochemistry, Geophysics, Geosystems*, *25*(1). https://doi.org/10.1029/2023GC011049

Arndt, I., Bernecker, M., Erhardt, T., Evans, D., Fiebig, J., Fursman, M., Kniest, J., Renema, W., Schlidt, V., Staudigel, P., Voigt, S., & Müller, W. (2025). 20,000 days in the life of a giant clam reveal late Miocene tropical climate variability. *Palaeogeography, Palaeoclimatology, Palaeoecology*, *661*. https://doi.org/10.1016/j.palaeo.2024.112711

Bajnai, D., Guo, W., Spötl, C., Coplen, T. B., Methner, K., Löffler, N., Krsnik, E., Gischler, E., Hansen, M., Henkel, D., Price, G. D., Raddatz, J., Scholz, D., & Fiebig, J. (2020). Dual clumped isotope thermometry resolves kinetic biases in carbonate formation temperatures. *Nature Communications*, *11*(1). https://doi.org/10.1038/s41467-020-17501-0

Bernasconi, S. M., Daëron, M., Bergmann, K. D., Bonifacie, M., Meckler, A. N., Affek, H. P., Anderson, N., Bajnai, D., Barkan, E., Beverly, E., Blamart, D., Burgener, L., Calmels, D., Chaduteau, C., Clog, M., Davidheiser-Kroll, B., Davies, A., Dux, F., Eiler, J., … Ziegler, M. (2021). InterCarb: A Community Effort to Improve Interlaboratory Standardization of the Carbonate Clumped Isotope Thermometer Using Carbonate Standards. *Geochemistry, Geophysics, Geosystems*, *22*(5). https://doi.org/10.1029/2020GC009588

Bernasconi, S. M., Müller, I. A., Bergmann, K. D., Breitenbach, S. F. M., Fernandez, A., Hodell, D. A., Jaggi, M., Meckler, A. N., Millan, I., & Ziegler, M. (2018). Reducing Uncertainties in Carbonate Clumped Isotope Analysis Through Consistent Carbonate-Based Standardization. *Geochemistry, Geophysics, Geosystems*, *19*(9), 2895–2914. https://doi.org/10.1029/2017GC007385

Bernecker, M., Hofmann, S., Staudigel, P. T., Davies, A. J., Tagliavento, M., Meijer, N., Ballian, A., & Fiebig, J. (2023). A robust methodology for triple (Δ47, Δ48, Δ49) clumped isotope analysis of carbonates. *Chemical Geology*, *642*, 121803. https://doi.org/10.1016/j.chemgeo.2023.121803

Bigeleisen, J. (1965). Chemistry of Isotopes. *Science*, *147*(3657), 463–471. https://doi.org/10.1126/science.147.3657.463

Bonifacie, M., Calmels, D., Eiler, J. M., Horita, J., Chaduteau, C., Vasconcelos, C., Agrinier, P., Katz, A., Passey, B. H., Ferry, J. M., & Bourrand, J. J. (2017). Calibration of the dolomite clumped isotope thermometer from 25 to 350 °C, and implications for a universal calibration for all (Ca, Mg, Fe)CO3 carbonates. *Geochimica et Cosmochimica Acta*, *200*, 255–279. https://doi.org/10.1016/j.gca.2016.11.028

Böttcher, M. E. (1996). 18O/16O and 13C/12C fractionation during the reaction of carbonates with phosphoric acid effects of cationic substitution and reaction temperature. *Isotopes in Environmental and Health Studies*, *32*(2–3), 299–305. https://doi.org/10.1080/10256019608036323

Came, R. E., Eiler, J. M., Veizer, J., Azmy, K., Brand, U., & Weidman, C. R. (2007). Coupling of surface temperatures and atmospheric CO2 concentrations during the Palaeozoic era. *Nature*, *449*(7159), 198–201. https://doi.org/10.1038/nature06085

Crouzet, C., Brunet, F., Recham, N., Findling, N., Lanson, M., Guyot, F., Ferrasse, J. H., & Goffé, B. (2017). Hydrogen production by hydrothermal oxidation of FeO under acidic conditions. *International Journal of Hydrogen Energy*, *42*(2), 795–806. https://doi.org/10.1016/j.ijhydene.2016.10.019

Daëron, M. (2021). Full Propagation of Analytical Uncertainties in Δ47 Measurements. *Geochemistry, Geophysics, Geosystems*, *22*(5). https://doi.org/10.1029/2020GC009592

Daëron, M., Blamart, D., Peral, M., & Affek, H. P. (2016). Absolute isotopic abundance ratios and the accuracy of Δ47 measurements. *Chemical Geology*, *442*, 83–96. https://doi.org/10.1016/j.chemgeo.2016.08.014

Daëron, M., & Vermeesch, P. (2024). Omnivariant Generalized Least Squares regression: Theory, geochronological applications, and making the case for reconciled Δ47 calibrations. *Chemical Geology*, *647*. https://doi.org/10.1016/j.chemgeo.2023.121881

Davies, A. J., Brand, U., Tagliavento, M., Bitner, M. A., Bajnai, D., Staudigel, P., Bernecker, M., & Fiebig, J. (2023). Isotopic disequilibrium in brachiopods disentangled with dual clumped isotope thermometry. *Geochimica et Cosmochimica Acta*. https://doi.org/10.1016/j.gca.2023.08.005

Davies, A. J., Guo, W., Bernecker, M., Tagliavento, M., Raddatz, J., Gischler, E., Flögel, S., & Fiebig, J. (2022). Dual clumped isotope thermometry of coral carbonate. *Geochimica et Cosmochimica Acta*, *338*, 66–78. https://doi.org/10.1016/j.gca.2022.10.015

de Winter, N. J., Witbaard, R., Kocken, I. J., Müller, I. A., Guo, J., Goudsmit, B., & Ziegler, M. (2022). Temperature Dependence of Clumped Isotopes (Δ47) in Aragonite. *Geophysical Research Letters*, *49*(20). https://doi.org/10.1029/2022GL099479

Defliese, W. F., Hren, M. T., & Lohmann, K. C. (2015). Compositional and temperature effects of phosphoric acid fractionation on δ47 analysis and implications for discrepant calibrations. *Chemical Geology*, *396*, 51–60. https://doi.org/10.1016/j.chemgeo.2014.12.018

Dennis, K. J., Affek, H. P., Passey, B. H., Schrag, D. P., & Eiler, J. M. (2011). Defining an absolute reference frame for 'clumped' isotope studies of CO2. *Geochimica et Cosmochimica Acta*, *75*(22), 7117–7131. https://doi.org/10.1016/j.gca.2011.09.025

Fernandez, A., Tang, J., & Rosenheim, B. E. (2014). Siderite 'clumped' isotope thermometry: A new paleoclimate proxy for humid continental environments. *Geochimica et Cosmochimica Acta*, *126*, 411–421. https://doi.org/10.1016/j.gca.2013.11.006

Fiebig, J., Bajnai, D., Löffler, N., Methner, K., Krsnik, E., Mulch, A., & Hofmann, S. (2019). Combined high-precision Δ48 and Δ47 analysis of carbonates. *Chemical Geology*, *522*, 186–191. https://doi.org/10.1016/j.chemgeo.2019.05.019

Fiebig, J., Bernecker, M., Meijer, N., Methner, K., Staudigel, P., Davies, A. J., Bayarjargal, L., Spahr, D., Winkler, B., Hofmann, S., Granzin, M., & Petersen, S. V. (2024). Carbonate clumped isotope values compromised by nitrate-derived NO2 interferent. *Chemical Geology*, 122382. https://doi.org/10.1016/j.chemgeo.2024.122382

Fiebig, J., Daëron, M., Bernecker, M., Guo, W., Schneider, G., Boch, R., Bernasconi, S. M., Jautzy, J., & Dietzel, M. (2021). Calibration of the dual clumped isotope thermometer for carbonates. *Geochimica et Cosmochimica Acta*. https://doi.org/10.1016/j.gca.2021.07.012

Fiebig, J., Hofmann, S., Löffler, N., Lüdecke, T., Methner, K., & Wacker, U. (2016). Slight pressure imbalances can affect accuracy and precision of dual inlet-based clumped isotope analysis. *Isotopes in Environmental and Health Studies*, *52*(1–2), 12–28. https://doi.org/10.1080/10256016.2015.1010531

Fosu, B. R., Jautzy, J. J., Yong, W., & Secco, R. A. (2023). Introducing the "Franken-Kiel" Carbonate Device: First Application to Δ47-T Calibrations of Calcite and Dolomite. *Geochemistry, Geophysics, Geosystems*, *24*(10). https://doi.org/10.1029/2023GC011047

Ghosh, P., Adkins, J., Affek, H., Balta, B., Guo, W., Schauble, E. A., Schrag, D., & Eiler, J. M. (2006). 13C-18O bonds in carbonate minerals: A new kind of paleothermometer. *Geochimica et Cosmochimica Acta*, *70*(6), 1439–1456. https://doi.org/10.1016/j.gca.2005.11.014

Ghosh, P., Eiler, J., Campana, S. E., & Feeney, R. F. (2007). Calibration of the carbonate 'clumped isotope' paleothermometer for otoliths>. *Geochimica et Cosmochimica Acta*, *71*(11), 2736–2744. https://doi.org/10.1016/j.gca.2007.03.015

Gilg, H. A., Struck, U., Vennemann, T., & Boni, M. (2003). Phosphoric acid fractionation factors for smithsonite and cerussite between 25 and 72°C. *Geochimica et Cosmochimica Acta*, *67*(21), 4049–4055. https://doi.org/10.1016/S0016-7037(03)00169-8

Guo, W., Mosenfelder, J. L., Goddard, W. A., & Eiler, J. M. (2009). Isotopic fractionations associated with phosphoric acid digestion of carbonate minerals: Insights from first-principles theoretical modeling and clumped isotope measurements. *Geochimica et Cosmochimica Acta*, *73*(24), 7203–7225. https://doi.org/10.1016/j.gca.2009.05.071

Henkes, G. A., Passey, B. H., Wanamaker, A. D., Grossman, E. L., Ambrose, W. G., & Carroll, M. L. (2013). Carbonate clumped isotope compositions of modern marine mollusk and brachiopod shells. *Geochimica et Cosmochimica Acta*, *106*, 307–325. https://doi.org/10.1016/j.gca.2012.12.020

Holme, E. A., Henkes, G. A., Tosca, N. J., Rasbury, E. T., Young, J. M., Schaub, D. R., Nekvasil, H., & Hurowitz, J. A. (2023). Experimental constraints on siderite clumped isotope thermometry. *Geochimica et Cosmochimica Acta*, *343*, 323–340. https://doi.org/10.1016/j.gca.2022.12.012

Horita, J. (2014). Oxygen and carbon isotope fractionation in the system dolomite-water-CO2 to elevated temperatures. *Geochimica et Cosmochimica Acta*, *129*, 111–124. https://doi.org/10.1016/j.gca.2013.12.027

Hu, B., Gao, J., Fan, C., Li, Y., Qin, Y., Zhao, Y., & Tian, Y. (2019). Impact of nitrate contamination on the analysis of carbon and oxygen isotopes in carbonate and a low-temperature phosphoric acid digestion approach for online sample preparation. *Rapid Communications in Mass Spectrometry*, *33*(1), 12–20. https://doi.org/10.1002/rcm.8289

Kele, S., Breitenbach, S. F. M., Capezzuoli, E., Meckler, A. N., Ziegler, M., Millan, I. M., Kluge, T., Deák, J., Hanselmann, K., John, C. M., Yan, H., Liu, Z., & Bernasconi, S. M. (2015). Temperature dependence of oxygen- and clumped isotope fractionation in carbonates:

A study of travertines and tufas in the 6-95°C temperature range. *Geochimica et Cosmochimica Acta*, *168*, 172–192. https://doi.org/10.1016/j.gca.2015.06.032

Kelson, J. R., Huntington, K. W., Schauer, A. J., Saenger, C., & Lechler, A. R. (2017). Toward a universal carbonate clumped isotope calibration: Diverse synthesis and preparatory methods suggest a single temperature relationship. *Geochimica et Cosmochimica Acta*, *197*, 104–131. https://doi.org/10.1016/j.gca.2016.10.010

Kim, S. T., O'Neil, J. R., Hillaire-Marcel, C., & Mucci, A. (2007). Oxygen isotope fractionation between synthetic aragonite and water: Influence of temperature and Mg2+ concentration. *Geochimica et Cosmochimica Acta*, *71*(19), 4704–4715. https://doi.org/10.1016/j.gca.2007.04.019

Kim, S.-T., & O'Neil, J. R. (1997). Equilibrium and nonequilibrium oxygen isotope effects in synthetic carbonates. *Geochimica et Cosmochimica Acta*, *61*(16), 3461–3475. https://doi.org/10.1016/S0016-7037(97)00169-5

Kluge, T., John, C. M., Jourdan, A. L., Davis, S., & Crawshaw, J. (2015). Laboratory calibration of the calcium carbonate clumped isotope thermometer in the 25-250°C temperature range. *Geochimica et Cosmochimica Acta*, *157*, 213–227. https://doi.org/10.1016/j.gca.2015.02.028

Kniest, J. F., Davies, A. J., Brugger, J., Fiebig, J., Bernecker, M., Todd, J. A., Hickler, T., Voigt, S., Woodland, A., & Raddatz, J. (2024). Dual clumped isotopes from Mid-Eocene bivalve shell reveal a hot and summer wet climate of the Paris Basin. *Communications Earth and Environment*, *5*(1). https://doi.org/10.1038/s43247-024-01491-8

Kong, K., Guo, Y., Deng, W., & Wei, G. (2023). Synthetic Witherite for Standardisation of Clumped Isotope (Δ47) Measurements. *Geostandards and Geoanalytical Research*, *47*(4), 855–868. https://doi.org/10.1111/ggr.12520

Kříbek, B., Knésl, I., Rojík, P., Sýkorová, I., & Martínek, K. (2017). Geochemical history of a Lower Miocene lake, the Cypris Formation, Sokolov Basin, Czech Republic. *Journal of Paleolimnology*, *58*(2), 169–190. https://doi.org/10.1007/s10933-017-9970-2

Kruskal, W. H., & Wallis, W. A. (1952). Use of Ranks in One-Criterion Variance Analysis. In *Source: Journal of the American Statistical Association* (Vol. 47, Issue 260).

Lafuente, B., Downs, R. T., Yang, H., & Stone, N. (2015). 1. The power of databases: The RRUFF project. In *Highlights in Mineralogical Crystallography* (pp. 1–30). DE GRUYTER. https://doi.org/10.1515/9783110417104-003

Lebeau, O., Busigny, V., Chaduteau, C., & Ader, M. (2014). Organic matter removal for the analysis of carbon and oxygen isotope compositions of siderite. *Chemical Geology*, *372*, 54–61. https://doi.org/10.1016/j.chemgeo.2014.02.020

Lu, C., Murray, S. T., Klaus, J., McNeill, D. F., & Swart, P. K. (2024). Dual clumped isotopes (Δ47 and Δ48) reveal non-equilibrium formation of freshwater cements. *Geochimica et Cosmochimica Acta*, *379*, 145–157. https://doi.org/10.1016/j.gca.2024.06.037

Lu, C., Zou, H., Wang, G., Cong, F., Quan, Y., & Swart, P. K. (2023). Clumped isotopes of paired dolomite and calcite constraining alteration histories of ancient carbonate successions. *Chemical Geology*, *617*. https://doi.org/10.1016/j.chemgeo.2022.121264

Mann, H. B., & Whitney, D. R. (1947). On a Test of Whether one of Two Random Variables is Stochastically Larger than the Other. *The Annals of Mathematical Statistics*, *18*(1), 50–60. https://doi.org/10.1214/aoms/1177730491

McCrea, J. M. (1950). On the isotopic chemistry of carbonates and a paleotemperature scale. *The Journal of Chemical Physics*, *18*(6), 849–857. https://doi.org/10.1063/1.1747785

Müller, I. A., Rodriguez-Blanco, J. D., Storck, J. C., do Nascimento, G. S., Bontognali, T. R. R., Vasconcelos, C., Benning, L. G., & Bernasconi, S. M. (2019). Calibration of the oxygen and clumped isotope thermometers for (proto-)dolomite based on synthetic and natural carbonates. *Chemical Geology*, *525*, 1–17. https://doi.org/10.1016/j.chemgeo.2019.07.014

Müller, I. A., Violay, M. E. S., Storck, J. C., Fernandez, A., van Dijk, J., Madonna, C., & Bernasconi, S. M. (2017). Clumped isotope fractionation during phosphoric acid digestion of carbonates at 70 °C. *Chemical Geology*, *449*, 1–14. https://doi.org/10.1016/j.chemgeo.2016.11.030

Parvez, Z. A., Lucarelli, J. K., Matamoros, I. W., Rubi, J., Miguel, K., Elliott, B., Flores, R., Ulrich, R. N., Eagle, R. A., Watkins, J. M., Christensen, J. N., & Tripati, A. (2023). Dual carbonate clumped isotopes (Δ47-Δ48) constrains kinetic effects and timescales in peridotite-associated springs at the Cedars, Northern California. *Geochimica et Cosmochimica Acta*, *358*, 77–92. https://doi.org/10.1016/j.gca.2023.06.022

Passey, B. H., & Henkes, G. A. (2012). Carbonate clumped isotope bond reordering and geospeedometry. *Earth and Planetary Science Letters*, *351–352*, 223–236. https://doi.org/10.1016/j.epsl.2012.07.021

Passey, B. H., Levin, N. E., Cerling, T. E., Brown, F. H., & Eiler, J. M. (2010). High-temperature environments of human evolution in East Africa based on bond ordering in paleosol carbonates. *Proceedings of the National Academy of Sciences of the United States of America*, *107*(25), 11245–11249. https://doi.org/10.1073/pnas.1001824107

Petersen, S. V., Defliese, W. F., Saenger, C., Daëron, M., Huntington, K. W., John, C. M., Kelson, J. R., Bernasconi, S. M., Colman, A. S., Kluge, T., Olack, G. A., Schauer, A. J., Bajnai, D., Bonifacie, M., Breitenbach, S. F. M., Fiebig, J., Fernandez, A. B., Henkes, G. A., Hodell, D., … Winkelstern, I. Z. (2019). Effects of Improved 17O Correction on Interlaboratory Agreement in Clumped Isotope Calibrations, Estimates of Mineral-Specific Offsets, and Temperature Dependence of Acid Digestion Fractionation. *Geochemistry, Geophysics, Geosystems*, *20*(7), 3495–3519. https://doi.org/10.1029/2018GC008127

Rojik, P. (2004). Journal of geosciences. *Journal of the Czech Geological Society*, *49*(3–4), 173–185. http://www.jgeosci.org/detail/JCGS.969

Rosenbaum, J., & Sheppard, S. M. F. (1986). An isotopic study of siderites, dolomites and ankerites at high temperatures. *Geochimica et Cosmochimica Acta*, *50*(6), 1147–1150. https://doi.org/10.1016/0016-7037(86)90396-0

Schauble, E. A., Ghosh, P., & Eiler, J. M. (2006). Preferential formation of 13C-18O bonds in carbonate minerals, estimated using first-principles lattice dynamics. *Geochimica et Cosmochimica Acta*, *70*(10), 2510–2529. https://doi.org/10.1016/j.gca.2006.02.011

Schauer, A. J., Kelson, J., Saenger, C., & Huntington, K. W. (2016). Choice of 17O correction affects clumped isotope (Δ47) values of CO2 measured with mass spectrometry. *Rapid Communications in Mass Spectrometry*, *30*(24), 2607–2616. https://doi.org/10.1002/rcm.7743

Sharma, T., & Clayton, R. N. (1965). Measurement of ratios of total oxygen of carbonates. *Geochimica et Cosmochimica Acta*, *29*(12), 1347–1353. https://doi.org/10.1016/0016-7037(65)90011-6

Siebert, J., Corgne, A., & Ryerson, F. J. (2011). Systematics of metal-silicate partitioning for many siderophile elements applied to Earth's core formation. *Geochimica et Cosmochimica Acta*, *75*(6), 1451–1489. https://doi.org/10.1016/j.gca.2010.12.013

946 Staudigel, P., Feng, D., Peckmann, J., Bernecker, M., Davies, A., Tagliavento, M., & Fiebig, J.
947 (2024). Resolving and correcting for kinetic biases on methane seep paleotemperature
948 using carbonate Δ_{47}/Δ_{48} analysis. *Science Advances*, *10*(22), 155.
949 https://doi.org/10.1126/sciadv.adn0155
950 Staudigel, P. T., & Swart, P. K. (2018). A Kinetic Difference Between 12C- and 13C-Bound
951 Oxygen Exchange Rates Results in Decoupled δ18O and Δ47 Values of Equilibrating DIC
952 Solutions. *Geochemistry, Geophysics, Geosystems*, *19*(8), 2371–2383.
953 https://doi.org/10.1029/2018GC007500
954 Swart, P. K., Burns, S. J., & Leder, J. J. (1991). Fractionation of the stable isotopes of oxygen
955 and carbon in carbon dioxide during the reaction of calcite with phosphoric acid as a
956 function of temperature and technique. *Chemical Geology: Isotope Geoscience Section*,
957 *86*(2), 89–96. https://doi.org/10.1016/0168-9622(91)90055-2
958 Tagliavento, M., Davies, A. J., Bernecker, M., Staudigel, P. T., Dawson, R. R., Dietzel, M.,
959 Götschl, K., Guo, W., Schulp, A. S., Therrien, F., Zelenitsky, D. K., Gerdes, A., Müller, W.,
960 & Fiebig, J. (2023). Evidence for heterothermic endothermy and reptile-like eggshell
961 mineralization in Troodon, a non-avian maniraptoran theropod. *Proceedings of the*
962 *National Academy of Sciences of the United States of America*, *120*(15).
963 https://doi.org/10.1073/pnas.2213987120
964 Tang, J., Dietzel, M., Fernandez, A., Tripati, A. K., & Rosenheim, B. E. (2014). Evaluation of
965 kinetic effects on clumped isotope fractionation (δ47) during inorganic calcite
966 precipitation. *Geochimica et Cosmochimica Acta*, *134*, 120–136.
967 https://doi.org/10.1016/j.gca.2014.03.005
968 Tripati, A. K., Eagle, R. A., Thiagarajan, N., Gagnon, A. C., Bauch, H., Halloran, P. R., & Eiler, J.
969 M. (2010). 13C-18O isotope signatures and 'clumped isotope' thermometry in
970 foraminifera and coccoliths. *Geochimica et Cosmochimica Acta*, *74*(20), 5697–5717.
971 https://doi.org/10.1016/j.gca.2010.07.006
972 Tripati, A. K., Hill, P. S., Eagle, R. A., Mosenfelder, J. L., Tang, J., Schauble, E. A., Eiler, J. M.,
973 Zeebe, R. E., Uchikawa, J., Coplen, T. B., Ries, J. B., & Henry, D. (2015). Beyond
974 temperature: Clumped isotope signatures in dissolved inorganic carbon species and the
975 influence of solution chemistry on carbonate mineral composition. *Geochimica et*
976 *Cosmochimica Acta*, *166*, 344–371. https://doi.org/10.1016/j.gca.2015.06.021
977 Uchikawa, J., Chen, S., Eiler, J. M., Adkins, J. F., & Zeebe, R. E. (2021). Trajectory and timescale
978 of oxygen and clumped isotope equilibration in the dissolved carbonate system under
979 normal and enzymatically-catalyzed conditions at 25 °C. *Geochimica et Cosmochimica*
980 *Acta*, *314*, 313–333. https://doi.org/10.1016/j.gca.2021.08.014
981 Urey, H. C. (1947). The thermodynamic properties of isotopic substances. *Journal of the*
982 *Chemical Society (Resumed)*, 562. https://doi.org/10.1039/jr9470000562
983 Wacker, U., Fiebig, J., & Schoene, B. R. (2013). Clumped isotope analysis of carbonates:
984 comparison of two different acid digestion techniques. *Rapid Communications in Mass*
985 *Spectrometry*, *27*(14), 1631–1642. https://doi.org/10.1002/rcm.6609
986 Walters, L. J., Claypool, G. E., & Choquette, P. W. (1972). Reaction rates and SO1* variation
987 for the carbonate-phosphoric acid preparation method. *Geochimica et Cosmochimica*
988 *Acta*, *36*, 129–140.
989 Wang, Z., Schauble, E. A., & Eiler, J. M. (2004). Equilibrium thermodynamics of multiply
990 substituted isotopologues of molecular gases. *Geochimica et Cosmochimica Acta*, *68*(23),
991 4779–4797. https://doi.org/10.1016/j.gca.2004.05.039

992 Wendeberg, M., Richter, J. M., Rothe, M., & Brand, W. A. (2011). δ18O anchoring to VPDB:
993 Calcite digestion with 18O-adjusted ortho-phosphoric acid. *Rapid Communications in*
994 *Mass Spectrometry*, *25*(7), 851–860. https://doi.org/10.1002/rcm.4933
995 Winkelstern, I. Z., Kaczmarek, S. E., Lohmann, K. C., & Humphrey, J. D. (2016). Calibration of
996 dolomite clumped isotope thermometry. *Chemical Geology*, *443*, 32–38.
997 https://doi.org/10.1016/j.chemgeo.2016.09.021
998 Zimmerman, D. W. (2000). Statistical significance levels of nonparametric tests biased by
999 heterogeneous variances of treatment groups. *Journal of General Psychology*, *127*(4),
1000 354–364. https://doi.org/10.1080/00221300009598589
1001